Republic of Iraq
Ministry of Higher Education
And Scientific Research
University of Thi-Qar
College of Science



Electronic structure and electron transport properties of double mesoscopic ring

A Thesis Submitted to the College of Science University of Thi-Qar in Partial Fulfillment of the Requirements for the Degree of Master of Science in Physics

By

Samar Mizher Mirdas

B.Sc.in Physics Thi-Qar 2010

Supervised by

Assist.Prof.Lafy Faraj Al-Badry

Prof.Dr.Falah Hasan Hanoon

2018 A.D.

1439 H.D

بسم الله الرحمن الرحيم

وَلَسَوْفَ يُعْطِيكَ رَبُّكَ فَتَرْضَىٰٓ

صدق الله العلي العظيم

سورة الضحى الأية (٥)

Certificate

We Certify that the preparation of thesis entitled ***(Electronic structure and electron transport properties of double mesoscopic ring)*** was made under our supervision by ***Samar Mizher Mirdas*** at the department of physics, college of science, Thi-Qar university as a partial requirement for the degree of master of science in physics.

Signature:

Name: Dr.Lafy Faraj Al-Badry

Title: Assistant professor

Date: / / 2018

Signature:

Name: Dr.Falah Hasan Hanoon

Title: professor

Date: / / 2018

In view of the available recommendations, I forward this thesis for debate by examining committee.

Signature:

Name: Dr. Emad Abdul-Razaq Salman

Title: Assistant professor

Head of physics Department College of Science / Thi-Qar University

Date: / / 2018

Dedication

To My Imam

To My Father and Mother

To My Brothers and Sisters

Samar

Acknowledgments

All Praise is due to Allah lord of the world, and best prayers and peace be unto his best messenger Mohammed, and his pure descendants, and his noble companions.

Then, I would like to express my deep gratitude and appreciation to my supervisor, Assist. Prof. Dr. Lafy Faraj Al-Badry and Prof. Dr. Falah Hasan Hanoon for suggesting the topic of the thesis to me, and for his continuous advice and his guidance throughout this work.

I would like to express my deep thanks to dean of the college of science and the chairman of physics department for their help.

Finally, I would like to thank all members of my family for their help and encouragement and everyone who helped me during the preparation of this thesis.

Samar

List of symbols

Symbols	Meaning
E	Total energy
L_f	The phase coherence length
τ_D	The diffusion time
τ_{in}	The inelastic scattering time
Z_g	The grand canonical partition function
M	Magnetization
R	The radius
$f(E_n)$	Fermi factor
$\sigma(\omega)$	dynamical electrical conductivity
$E_m(k)$	The dispersion relation
$n_m(k)$	The occupation number for the quantum state
$E_0(\Phi)$	The ground state energy
μ	Chemical potential
N	Number of atomic sites
k_B	Boltzmann constant
ϕ	Phase factor
Φ	Magnetic flux

Φ_0	Flux quantum
T	Temperature
H	Hamiltonian
e	Electron charge
S	Surface area
χ	Electronegativity
ω	Electrophilicity
η	Electrochemical Hardness
ρ	Resistivity
t_{up}	Nearest-neighbor hopping strength of upper rings
t_{lo}	Nearest-neighbor hopping strength of lower rings
E_{up}	The on-site energies of upper rings
E_{lo}	The on-site energies of lower rings
$\mathcal{M}$	Magnetic moment
$\chi(\Phi)$	Susceptibility
I	Persistent current
D	Drude weight
V	Inter-ring coupling strength
Φ_t	Transverse flux

T(E)	Transmission probability
$\Delta\varphi$	The phase shift difference between the upper and lower arms of ring
$c_{ij}^{\dagger}(c_{ij})$	represent the creation (annihilation) operators
$\sigma_{reg}(\omega)$	The regular part of the conductivity
$\delta(\omega)$	Singular contribution
E_g	Energy gap
E_F	Fermi energy

List of Abbreviations

Attribute	Meaning
DFT	Density Functional Theory
DOS	Density Of States
2DEG	2-dimension electron gass
E.A	Electron Affinity
G09	Gaussian 2009 Version
HOMO	High Occupied Molecular
LUMO	Low Unoccupied Molecular Orbital
I.P	Ionization Potential
IR	Infrared Spectra
Inc	Incorporation

Abstract

The present work is a theoretical study of the electronic properties of double mesoscopic ring threaded by Aharonov-Bohm flux. The system that takes into account in the study is consisting of two rings connected in parallel, with two different types of atomic sites.

This work contains two parts. First part is analytical study of the energy spectrum, persistent current, Drude weight and low-field magnetic susceptibility of double mesoscopic ring by tight-binding method. Electronic properties are calculated with and without transverse flux. Analytical results show that the on-site energies for both types of atoms, inter-ring coupling, nearest-neighbor hopping strengths and transverse flux play an important role in controlling the electronic properties of the studied system.

The second part is a simulation and completion of the electronic properties studied in the first part. This part consider as computational study for electronic properties of metallic rings in their ground electronic states by density functional theory (DFT), which achieved with standard Gaussian 09W software package. The studied metallic rings in second part are single metal ring, pristine double metal ring and alloyed double metal ring of noble metals Au, Cu and Ag. Single metallic ring formed with the number of atoms (3-6). The pristine double metal ring designed from two rings with same metal, each ring contains 6 atoms. While alloyed double metallic ring designed from two rings with dissimilar metals. The best geometry, HOMO, LUMO, energy gap, electronegativity, electrophilicity, chemical hardness and chemical softness show that the studied systems have semiconductor characteristic.

Contents:

No	Subject	Page
	Chapter 1: Fundamentals	
1.1	Introduction	1
1.2	Quantum rings	3
1.3	Persistent current	4
1.4	Magnetization	6
1.5	Drude weight	8
1.6	Aharonov-Bohm effect	9
1.7	Literature Review	10
1.8	Aim of the study	14
1.9	Thesis outline	14
	Chapter 2: Theoretical Model	
2.1	Introduction	16
2.2	Theoretical Model	17
2.3	Energy spectrum	18
2.4	Persistent current	20
2.5	Drude weight	21

2.6	Low-field magnetic susceptibility	22
Chapter 3: Result and Discussion		
3.1	Energy spectrum in absence transverse magnetic flux	24
3.2	Persistent current	25
3.3	Drude weight	28
3.4	Low-field magnetic susceptibility	28
3.5	Energy spectrum with presence transverse magnetic flux	29
Chapter 4: Density Functional Theory Calculations		
4.1	Introduction	44
4.2	Computational Details	45
4.3	Computational Results	46
4.3.1	Equilibrium geometries	46
4.3.2	Frontier Orbital Energies	47
4.3.3	Global Reactivity Descriptors	49
Chapter 5: Conclusions and Future Works		
5.1	Conclusions	61
5.2	Future works	62
References		

Chapter One

Fundamentals

1-1 Introduction

Over the last few decades the effect of persistent current in mesoscopic ring systems has received much attention because its important role in understanding quantum coherence in such ring systems [1]. Quantum interference phenomena have been revealed in mesoscopic ring systems exposed of a magnetic flux, such as the Aharonov-Bohm effect in the persistent currents, which never decay with time[2].

Mesoscopic ring systems must have two important characteristics to obtain persistent current. The first, the size of the system must be comparable to the phase coherence length of electrons. The second, the system must be at sufficiently low temperature. These two conditions arise from the fact that the average energy level spacing must be greater than the thermal energy. The average energy level spacing increases as the size of the system decreases, therefore, the persistent current will flow in the mesoscopic ring systems. As a result, the discrete of energy levels plays important role in the flow persistent currents in mesoscopic rings [2-4].

With the advance in nanoscience and nanotechnology it has been possible to fabricate structures whose sizes are much smaller than the mean free path of an electron. The phase coherence length L_f of the electrons in mesoscopic systems is larger than the system size L at very low temperature, and hence the electron transport is completely phase coherent. The transport phenomena

in such low-dimensional systems give several novel and interesting new results [5].

The phenomenon of persistent current in mesoscopic rings threaded by an magnetic flux Φ has been based over many decades. The presence of large phase coherence length and discrete energy levels allow persistent current upon the application of an external magnetic flux Φ [6].

The existence of dissipationless current, the so-called persistent current, in a mesoscopic normal metal ring pierced by an AB flux-is one of such remarkable effects which shows the significance of phase coherence of electronic waves in mesoscopic systems [7].

The persistent current is mean an electrical current flowing around a ring which is constant in time and which is not driven by a power source external to the ring. This current arises from the fact that for any disorder configuration of the ring each energy eigenstate possesses a non-zero expectation value for its angular momentum. Angular momentum of electron has a current associated with it, because the electron is a charged particle. These eigenstates with finite angular momentum are analogous to the eigenstates of an electron orbiting a nucleus which also possess finite angular momenta for electrons outside of the s-orbital[8].

In principle, the calculation of the current in a ring of many electrons boils down to calculating the current associated with each energy eigenstate and then summing up each of these currents with an appropriate weighting factor reflecting the thermal population of that state. While persistent currents are usually associated with superconductors and atomic and molecular quantum

systems, quantum mechanics allows, surprisingly, for such a current to exist in a resistive material as well. For the persistent current in a ring of resistive material to be measurable, the ring must be cold ($\leq 1K$) and small($\leq 1\mu m$) [8]. The behavior of persistent current in mesoscopic ring threading a magnetic flux is highly sensitive to the location of Fermi level of the system where the role of magnetic flux is essentially to destroy the time-reversal symmetry and as a result, the degeneracies among the current-carrying states get removed. Depending on the Fermi level and the direction of the magnetic flux, current flows in either direction revealing diamagnetic or paramagnetic nature [9].

1-2 Quantum rings

Nanoscale conducting rings, which are now commonly called Aharonov-Bohm quantum rings, are among other quantum systems used for experimental studies of the renowned discovery. Few-electron quantum rings with a radial size of $10 - 20$nm are now easily fabricated. The mean free path of particles confined in these nanostructures exceeds the ring length, which results in the quantum interference effects experienced by particles, in simillar to superconducting quantum interference devices (SQUIDs). The influence of the field potentials upon this interference in the regions with vanishing field magnitudes is direct evidence of the Aharonov-Bohm effect present in quantum rings [10, 11].

The interference phenomena occur even in rather large disordered samples described as microscopic, that are found between the microscopic and macroscopic structures according to size. They are at the crossover from the

quantum mechanical to the classical regime. The phase-coherence length of the electrons can be measured. At a given temperature in a given material the phase-coherence length of the electrons is the circumference of the largest ring that reveals Aharonov-Bohm oscillations in its physical quantities. The phase-coherence length can be about a micron in normal metal rings at liquid helium temperature. At room temperature, the phase coherence length, which is roughly proportional to the inverse temperature, exceeds the circumference of a benzene molecule [12].

Another physical goal was to look at what happens if a magnetic field which penetrates the ring is switched on. If the vector potential is chosen such that the electrons on the ring are field-free but nevertheless there is a flux through the ring some interesting features like the Aharonov-Bohm effect and persistent currents periodic in flux occur [13].

Quantum rings a popular system in which one can investigate core aspects of quantum mechanics experimentally. The theoretical interest in ring systems has increased with the experimental advances and much of the theoretical work with nanorings is concerning rings pierced by a magnetic field. Such fields are often chosen to be zero at the perimeter of the ring (i.e. Aharonov-Bohm flux). Small rings subjected to these kind of magnetic fields generate what is called persistent currents, which are currents that do not diminish even if the ring contains impurities that in general would scatter the electrons [14].

1-3 Persistent current

The perpetual current flowing in small non superconducting rings without applied voltage under breaking of time reversal symmetry has been of great interest in theoretical and experimental physics over the last three decades.

Since the effect crucially depends on the coherence of the electron wave function over the whole ring it is a manifestation of a quantum mechanical effect in a mesoscopic system. The basic effect which can cause a persistent current in a resistive metal ring is physically closely related to the perpetual motion of an electron around the nucleus. Thus its presence was indeed stated in 1938 by Hund [15] and investigated for the case of a pristine system by Bloch [16] and Kulik [17]. However, the observation of the effect of a perpetual current flowing in a realistic normal metal ring containing elastic disorder stayed somewhat counterintuitive until Büttiker *et.al* [18] proposed in 1983 the existence of the effect even in those realistic mesoscopic systems.

Experimentally the persistent currents have been an interesting significance for several reasons. The currents are excessively small and using e.g. an ammeter would cause the electrons to lose phase coherence and destroy the effect. Therefore, one has to measure the small change in the magnetic moment produced by the currents instead. In addition, the rings have to be mesoscopically small, which means that the time it takes an electron to move around the ring - the so called diffusion time τ_D has to be smaller than the inelastic scattering time τ_{in}. And third, the effect is rapidly destroyed if the temperature goes up, which means that experiments have to be performed at one Kelvin and below [19].

In mesoscopic rings that are smaller than the phase coherence length of electrons, currents can permanently flow in metal ring, even if the metal is not in a superconducting case, under the condition that the ring threaded a magnetic flux. To exhibit these currents, the low temperature of system is necessary to decrease the probability of inelastic scattering from other

electrons and phonons, and the ring circumference must be sufficiently short such that phase coherence of the electrons is preserved around the ring [20].

When an external magnetic field is applied to a molecule, that its electrons are forced to move around the molecule, giving rise to a magnetically induced current density. According to Faraday's law, the induced current density induces in most molecules a magnetic field in the opposite direction to the external field. The effect of the external magnetic field on molecular systems is very similar to the effect of magnetic fields on a coil in classical physics [21].

1-4 Magnetization

The magnetization and persistent current are identical phenomena, but correspond to different sample geometries. The general characteristics of the magnetization can be studied in the geometry of an infinite plane placed in a uniform and a perpendicular magnetic field. Then persistent current considered to flowing in a ring threaded by an Aharonov–Bohm flux. A conductor placed in a uniform magnetic field B acquires a magnetic moment $\mathcal{M}$given by the derivative of the thermodynamic grand potential $\mathcal{G}(\mathrm{T},\mathrm{B},\mu) = -k_B T ln \mathrm{Z}_g$ with respect to the applied field [22].

$$\mathcal{M}(\mathrm{B}) = \left(\frac{\partial \mathcal{G}}{\partial B}\right)_{\mu,T} \qquad (1-1)$$

where Z_g is the grand canonical partition function, k_B is Boltzmann constant, T is temperature, μ is chemical potential. We define the magnetization M as the magnetic moment per unit volume and the magnetic susceptibility $\mathcal{X}$ as the linear response to a weak field [22] :

$$M = \frac{\mathcal{M}}{\Omega} \qquad (1-2)$$

$$\mathcal{X} = \lim_{B\to 0} \frac{d\mathrm{M}}{dB} \qquad (1-3)$$

For the specific case of a ring, the magnetic moment $\mathcal{M}$ is that of a current-carrying loop of area $S = \pi R^2$, where R the radius. The current $\mathrm{I} = \frac{\mathcal{M}}{\mathrm{S}}$ is best known as a persistent current, and it can be written in the form[22]:

$$I(\Phi) = \frac{\partial \mathcal{G}}{\partial \Phi} \qquad (1-4)$$

Where $\Phi = BS$ is the flux through the ring.

The persistent current will be simply obtained using the formal replacement of the magnetic moment $\mathcal{M}$ by the current I and of the magnetic field B by the fluxΦ. We start by studying the case of a non-interacting electron gas. The corresponding grand potential is a function of the single-particle energies E_n :

$$\mathcal{G} = -2k_B T \sum \ln(1 + e^{\beta(E_F - E_n)}) \qquad (1-5)$$

Where $\beta = \frac{1}{k_B T}$

Therefore, the magnetic moment at finite temperature is given by

$$\mathcal{M}(B) = -2\sum_n f(E_n)\frac{\partial E_n}{\partial B} \qquad (1-6)$$

The sum means contributions of each occupied level, where $f(E_n)$ is Fermi factor. The magnetic moment at zero temperature is,

$$\mathcal{M}(T=0,B) = -2\sum_{E_n<E_F}\frac{\partial E_n}{\partial B} \qquad (1-7)$$

The persistent current at finite and zero temperature can be written as,

$$I(\Phi) = -2\sum_n f(E_n)\frac{\partial E_n}{\partial \Phi} \qquad (1-8)$$

$$I(T=0,\Phi) = -2\sum_{E_n<E_F}\frac{\partial E_n}{\partial \Phi} \qquad (1-9)$$

1-5 Drude weight

The easiest accessible experimentally measurable transport quantity is the DC resistivity $\rho = \frac{1}{\sigma(0)}$ where $\sigma(\omega)$ denotes the dynamical electrical conductivity. The conductivity has been derived within linear response theory by Kubo. In systems with correlated electrons one has to take into account in addition to the regular part of the conductivity σ_{reg} also a singular contribution[12].

$$\sigma(\omega) = 2\pi D\delta(\omega) + \sigma_{reg}(\omega) \qquad (1-10)$$

where D represents the Drude weight. At zero temperature the Drude weight is the central quantity which determining the DC charge transport. As formulated by Kohn, the Drude weight-which is also called the charge stiffness-can be expressed as the second derivative of the ground-state energy with respect to the applied magnetics flux,

$$D = \frac{N}{4\pi^2}\frac{\partial^2 E_0}{\partial \phi^2}\Big|_{\phi=0} \qquad (1-11)$$

where N is the number of atoms in mesoscopic ring. A finite Drude weight is characteristic for a conductor or a metal. For an insulator, the Drude weight vanishes. At finite temperature, the Drude weight vanishes also for normal conductors. However, a finite Drude weight at finite temperature would be a signature of an ideal conductor, which does not show any energy dissipation. This case is realized by a number of nontrivial integrable many-fermion models. All integrable many-fermion models are one-dimensional[23].

Noteworthy the study of the Drude weight may not be useful for a very large system with disorder or strong interaction. For example, the strong on-site interaction could suppress the conductivity at half-filling for a large chain[24].

1-6 Aharonov-Bohm effect

In 1959, Aharonov and Bohm predicted that the partial waves of a charged particle enclosing an electrostatic or magnetic potential experience a magnetic phase shift, even if the magnetic and electric fields vanish in the regions of non-zero probability density. This phase should be distinguished from the dynamic phase, which is the frequency of the plane wave electronic states at the Fermi energy, integrated over time. Interferences as a function of the relative phase shift occur, which are known as the electrostatic and the magnetic Aharonov–Bohm (AB) effect, respectively [25].

Aharonov-Bohm (AB) effect became important in the field of low-dimensional semiconductor structures, which developed rapidly in the 1980s, which supply the industrial requirements of smaller and faster electronic devices. In 1985 first indications of the Aharonov–Bohm effect were observed in double-quantum well structures [26] and later also in semiconducting ring-shaped systems [27] also it was well studied in metallic systems [28] .

A ring is patterned out of a metal or a 2DEG, with a circumference smaller than the phase coherence length. Suppose a conducting ring encloses a magnetic vector potential $\vec{A}$ that generates a constant magnetic field vertical to the plane of the ring. The phase shift difference between the upper and lower arms of ring is given by [29].

$$\Delta\varphi = \frac{q}{\hbar}\oint \vec{A}\,.\,d\vec{l} \qquad (1-12)$$

$$\varphi_{up} - \varphi_{lo} = \frac{eBS}{\hbar} = \frac{2\pi\Phi}{\Phi_0} \qquad (1-13)$$

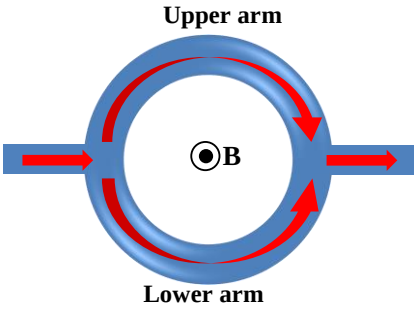


Fig. (1-1). A coherent semiconductor or metal ring attached to two metallic electrodes, a magnetic field perpendicularly applied on the ring.

where *S* is the surface area, Φ is magnetic flux. The total transmission probability T is obtained from**:**

$$T = 2{T_0}^2\left[1 + cos\left(\frac{2\pi\Phi}{\Phi_0}\right)\right] \qquad (1-14)$$

The phase $2\pi\Phi/\Phi_0$ is called the Aharonov–Bohm phase. Apparently, transmission probability oscillates as a function of magnetic field [30, 31].

1-7 Literature Review

1- In 2005, S. Gupta and *et al*. have investigated finite-sized single band Hubbard chains with Fibonacci modulation for half-filling case by using a mean field approximation. The ground state properties at zero and non-zero temperatures are calculated. They existed reduction in the conductivity due to strong electronic interaction or strong Fibonacci modulation [24].

2- In 2006, J. S. Sheng and K. Chang investigated theoretically spin states of electron in one-dimensional and two-dimensional (2D) hard-wall mesoscopic rings. They benefited from the presence of both the Rashba spin-orbit interaction (RSOI) and the Dresselhaus spinorbit interaction (DSOI) in a perpendicular magnetic field. They found for 2D ring with a finite width,

higher radial modes destroy the periodic oscillations of persistent currents [32].

3- In 2007, S. K. Maiti studied low-field magnetic susceptibility and persistent current in normal metal rings threaded by a magnetic flux. He has used tight-binding model for achieved all calculations in order and disorder ring. He has found in the rings described by fixed chemical potentials , the sign of the low-field currents cannot be predicted precisely [33].

4- In 2008, Bo. B. Wei and *et al*. studied persistent charge and spin currents in the ground state of the one-dimensional mesoscopic Hubbard ring. They used Bethe-ansatz solution. They discovered the persistent charge current is suppressed by the on-site Coulomb interaction more significantly at half-filling than non-half-filling and the persistent spin current is suppressed by the on-site Coulomb interaction, and it decays algebraically as the system size increases both at half-filling non -half-filling [34].

5- In 2010, M. Saha and S. K.Maiti studied disagreement between the measured and calculated current amplitudes carried by a small metal ring upon the application of an Aharonov-Bohm (AB) flux. He used Hartree-Fock (HF) approximation for calculate persistent current, Drude weight, low-field magnetic susceptibility and related issues. He found analysis may be inspiring for studying magnetic response in nano-scale loop geometries [35].

6- In 2011, S. K. Maiti and *et al*. studied transport properties of electrons in a mesoscopic ring threaded by a AB flux. The used a tight-binding formalism

for calculate persistent under effect Rashba and Dresselhaus spin-orbit interactions. They had observed that the presence of the spin-orbit interaction, leads to an enhanced amplitude of the persistent current [6].

7- In 2012, P. Dutta and *et al*. explored magneto-transport properties in a binary alloy ring exposed to an Aharonov- Bohm (AB) flux Φ within a tight-binding framework. They discussed two cases, the behavior of persistent current in an isolated order binary alloy ring as functions of electron concentration Ne and AB flux Φ. They managed the effect of impurities is also analyzed. They suggested the system can act as a p-type or an n-type semiconductor [36].

8- In 2013, M. A. Castellanos-Beltran and *et al*. analyzed the persistent current in individual normal metal rings over a wide range of magnetic fields. They found the sensitivity of persistent current to the mesoscopic fluctuations within a single isolated coherent volume [37].

9- In 2014, K. Bakke and C. Furtado investigated topological effects on the confinement of a moving particle with an induced electric dipole moment in a two-dimensional quantum dot and a quantum ring. They analyzed in this work that the spectrum of energy depends on the geometric phase obtained by Wei et al and they obtained persistent currents arise from this dependence in both the quantum ring and the quantum dot [38].

10- In 2015, S. Saha and *et al*. studied circular current in a single handed helical geometry threaded by magnetic flux φ. They used a Hartree-Fock

mean field approach. They discussed proximity effect between the sites which exhibits interesting results [2].

11- In 2016, M. Saha and S. K.Maiti studied persistent current of one-dimensional rings for different electron fillings in both ordered and disordered cases. They used exact diagonalization method of many-body Hamiltonian for compute eigenenergies. They found in half-filled case that a metal–insulator transition obtains by increasing correlation strength, but this behavior disappear in no half -filling case [39].

12- In 2017, C. Mckeever and *et al*. studied the high frequency dynamic behavior of concentric nanorings with vortex domain structures. They used micromagnetic simulations. They explained the ferromagnetic resonance of the concentric ring structure as a function of geometric parameters of the system [40].

13- In 2018, M. Filippone and *et al*. studied behavior of persistent currentsfor a limited number of noninteracting electrons in a quantum ladder exposed to Aharonov-Bohm and transverse magnetic fluxes. They explained that the coupling between ladder legs provides a way to effectively change the ground-state fermion-number parity by varyin transverse flux. They found that persistent currents appear a robust 4π periodicity as a function the number of sites [41].

1-8 Aim of the study

The aim of the present work is improvement of the persistent current in double mesoscopic ring in order to use in nanoelectronic devices. Calculate the other properties of the double mesoscopic ring that cannot be analytically calculated were evaluated by DFT method which achieved with standard Gaussian 09W software package. The electronic properties can be improved in order to obtain the best double mesoscopic ring that can provide the high persistent current. The process of improvement is done through the use of the pristine and alloyed double rings.

1-9 Thesis outline

The primary focus of this work is on the electronic properties of double mesoscopic ring. More clearly, an extended introduction concerned with electronic properties as well as a comprehensive survey of previous studies is presented in chapter one.

An expression for the tight-binding Hamiltonian and theoretical formula of energy spectrum, persistent current, Drude weight and low-field magnetic susceptibility have been derived. These formulations are presented in chapter two. In chapter three, the results of energy spectrum, persistent current, Drude weight and low-field magnetic susceptibility, in absence the transverse flux, are presented and discussed.

In chapter four, the density functional theory calculations are studied. The most important notes and future works are reported in chapter five.

Chapter two

Theoretical Model

2.1 Introduction

The enormous progresses of nanotechnology have allowed investigating electron transport in low-dimensional quantum systems. One of such systems is a mesoscopic ring which seems very simple, but has promising candidates from the application point of view. Many quantum phenomena have been appeared in this ring structures in presence of Aharonove-Bohm flux. One of quantum phenomena which observed in normal metal ring is persistent current. The long phase coherence length and discrete energy levels of mesoscopic ring allow persistent current in presence an external magnetic flux Φ. Persistent current is mean a constant electrical current with time flowing around a ring threaded by magnetic flux [36].

Now the study of magnetic properties in cylindrical systems and double mesoscopic rings is more realistic than the one-dimensional rings, because most of the traditional experiments are achieved in one-dimensional rings have finite width [5].

The tight-binding(TB) Hamiltonian is describing the system which comprises double mesoscopic ring with two different types of atoms. The ground state energy in presence Aharonov-Bohm flux evaluated from TB Hamiltonian, and which utilized to compute persistent current, Drude weight and magnetic susceptibility.

2-2 Theoretical Model

The considered system is illustrated in Fig. (2-1). A double mesoscopic ring, are vertically connected as cylinder. The upper and lower rings consist of two different types of atoms (a) and (b) with same the number of atomic sites. Both rings subjected to Aharonov-Bohm flux and transverse flux. The tight binding Hamiltonian of system is given by:

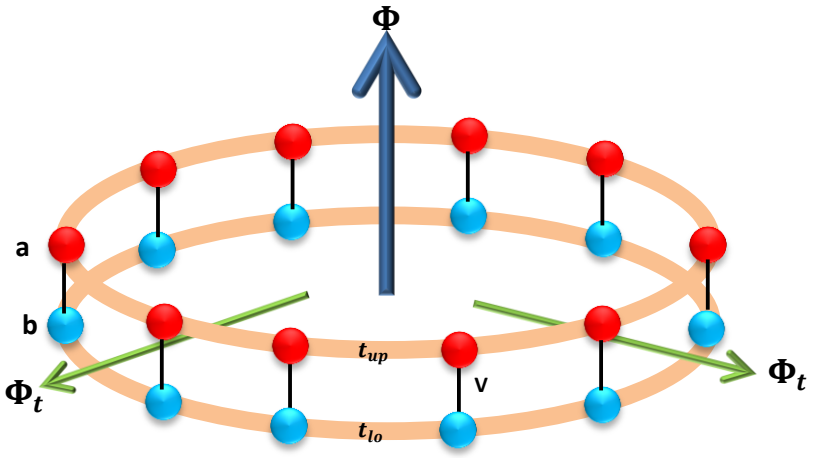


Fig. (2-1). Double mesoscopic ring threaded by Aharonov-Bohm flux Φ and transverse fluxΦ_t, a lower ring consists of one type of atomic sites different from atomic sites in upper ring.

$$H = E_{up}\sum_i a_i^\dagger a_i + E_{lo}\sum_j b_j^\dagger b_j - t_{up}\sum_i (a_i^\dagger a_{i+1} e^{i(\phi_{up}+\varphi_{up})} + h.c) - t_{lo}\sum_i (b_i^\dagger b_{i+1} e^{i(\phi_{lo}-\varphi_{lo})} + h.c) - V\sum_i (a_i^\dagger b_i + b_i^\dagger a_i) \qquad (2-1)$$

where, E_{up} and E_{lo} are the on-site energies of upper and lower rings, respectively, t_{up} and t_{lo} are the nearest-neighbor hopping strengths of upper and lower rings, respectively. While V is inter-ring coupling

strength. $a_i^\dagger(a_i)$ and $b_j^\dagger(b_j)$ represent the creation (annihilation) operators for an electron at the sites i and j, respectively. The phase factors of Aharonov-Bohm flux and transverse flux are $\phi_\alpha = \frac{2\pi}{N_\alpha}\frac{\Phi}{\Phi_0}$ and $\varphi_\alpha = \frac{\pi}{N_\alpha}\frac{\Phi_t}{\Phi_0}$, where α refers to upper and lower rings. Φ is magnetic flux generated by magnetic field applied in the vertical direction at the plane of the double mesoscopic ring, which called Aharonov-Bohm flux. While Φ_t is the magnetic flux exhibited by magnetic field applied in the radial direction, which called transverse flux, the number of atomic sites in each ring is N_α.

2-3 Energy spectrum

In order to calculate the energy dispersion relation for double mesoscopic ring let us begin with T.B Hamiltonian (2-1). By using Fourier transformation can be write creation and annihilation operators in k-space [42, 43]:

$$\sum_i a_i^\dagger\, a_i = \sum_k a_k^\dagger\, a_k \qquad (2-2)$$

$$\sum_j b_j^\dagger\, b_j = \sum_k b_k^\dagger\, b_k \qquad (2-3)$$

$$\sum_i a_i^\dagger\, b_i = \sum_k a_k^\dagger\, b_k\, e^{ika} \qquad (2-4)$$

$$\sum_i b_i^\dagger a_i = \sum_k b_k^\dagger a_k\, e^{-ika} \qquad (2-5)$$

$$\sum_i a_i^\dagger\, a_{i+1} = \sum_k a_k^\dagger\, a_k e^{ika} \qquad (2-6)$$

$$\sum_i b_i^\dagger\, b_{i+1} = \sum_k b_k^\dagger\, b_k e^{ika} \qquad (2-7)$$

where, a is the lattice constant and k is the wavevector is given by $\frac{2\pi n}{Na}$, n is a quantum number and it is confined within the rang $-\frac{N}{2} \leq n \leq \frac{N}{2}$ [36]. Therefore, the Hamiltonian can be transfer into the k-space by substituting the Eqs. (2-2)-(2-7) in Eq. (2-1)

$$H = \sum_k a_k^\dagger \, a_k \left(E_{up} - 2t_{up} \cos q_{up}\right) + \sum_k b_k^\dagger \, b_k (E_{lo} - 2t_{lo} \cos q_{lo}) - V \sum_k (a_k^\dagger \, b_k \, e^{ika} + b_k^\dagger a_k e^{-ika}) \qquad (2-8)$$

Where,

$$q_{up} = \frac{2\pi}{N_{up}} \left(n + \frac{\Phi}{\Phi_0} + \frac{1}{2}\frac{\Phi_t}{\Phi_0}\right) \qquad (2-9)$$

$$q_{lo} = \frac{2\pi}{N_{lo}} \left(n + \frac{\Phi}{\Phi_0} - \frac{1}{2}\frac{\Phi_t}{\Phi_0}\right) \qquad (2-10)$$

The Eq. (2-8) can be written as a matrix

$$H = \sum_k (a_k^\dagger \, , b_k^\dagger) \begin{pmatrix} E_{up} - 2t_{up} \cos q_{up} a & -Ve^{ika} \\ -Ve^{-ika} & E_{lo} - 2t_{lo} \cos q_{lo} a \end{pmatrix} \begin{pmatrix} a_k \\ b_k \end{pmatrix} \qquad (2-11)$$

The Hamiltonian can be written as matrix in the k space, for any tight-binding models have two quantum states per unit cell [44]:

$$H = \sum_k (c_k^\dagger \; d_k^\dagger) \begin{pmatrix} E_c & 0 \\ 0 & E_d \end{pmatrix} \begin{pmatrix} c_k \\ d_k \end{pmatrix} = \sum_k E_c \, (k) c_k^\dagger c_k + \sum_k E_d \, (k) d_k^\dagger d_k \qquad (2-12)$$

The total energy in k-space given by [45]:

$$E = \sum_{k,m} E_m(k)\, n_m\,(k)$$

$$= \sum_k E_1(k) n_1\,(k) + \sum_k E_2(k) n_2\,(k) \qquad (2-13)$$

where $E_m(k)$ and $n_m(k)$ are the energy dispersion relation and the occupation number for the quantum state in the mth band with momentum k, respectively. Therefore, in terms of Bloch waves the Hamiltonian should take the form

$$H = \sum_K E_1(k)\gamma_{1,k}^{\dagger}, \gamma_{1,k} + \sum_K E_2(k)\gamma_{2,k}^{\dagger}, \gamma_{2,k} \qquad (2-14)$$

where $\gamma_{n,k}^{\dagger}$ represents the creation operator for a Bloch wave in band n with momentum k. As we compare Eq. (2-14) with Eq. (2-12), two energy bands will occur. $c_k^{\dagger}$ and $d_k^{\dagger}$ creates a Bloch wave in two of the bands with momentum *k*. Therefore, the dispersion relations are written as:

$$E = \frac{(A+B) \pm \sqrt{(A-B)^2 + 4V^2}}{2} \qquad (2-15)$$

where

$$A = E_{up} - 2t_{up}\cos q_{up}a \qquad (2-16)$$

$$B = E_{lo} - 2t_{lo}\cos q_{lo}a \qquad (2-17)$$

2-4 Persistent current

At absolute zero temperature (T =0 K), the persistent current in the double mesoscopic ring described with fixed number of electrons N_e is determined by [3]:

$$I_n = -\frac{\partial E_0}{\partial \Phi} \qquad (2-18)$$

where $E_0(\Phi)$is the ground-state energy as a function of A-B fluxΦ [6]. By getting the energy eigenvalues as a function of flux Φ, the persistent current can be calculated for individual energy eigenstates. It is the first order derivative of energy as a function of flux. Therefore, the persistent current can be written for an n-th energy eigenstate as:

$$\mathrm{I_n} = -\frac{1}{2}\left[\left(\mathrm{X_{up}} + \mathrm{X_{lo}}\right) \pm \frac{\left(\mathrm{X_{up}} - \mathrm{X_{lo}}\right)(\mathrm{A} - \mathrm{B})}{\sqrt{(\mathrm{A} - \mathrm{B})^2 + 4\mathrm{V}^2}}\right] \qquad (2-19)$$

where,

$$X_{up} = t_{up}\frac{4\pi}{N_{up}\Phi_0} sin\frac{2\pi}{N_{up}}\left(n + \frac{\Phi}{\Phi_0} + \frac{1}{2}\frac{\Phi_t}{\Phi_0}\right) \qquad (2-20)$$

$$X_{lo} = t_{lo}\frac{4\pi}{N_{lo}\Phi_0} sin\frac{2\pi}{N_{lo}}\left(n + \frac{\Phi}{\Phi_0} - \frac{1}{2}\frac{\Phi_t}{\Phi_0}\right) \qquad (2-21)$$

where, +ve or −ve sign in Eq. (2-19) appears by depending on the choice of n i.e., which refers to sub-band the energy level, where $n = 0, \mp 1, \mp 2, \ldots$., The total persistent current I_T at absolute zero temperature for a particular filling N_e is performed by taking the sum of individual contributions of the lowest energy eigenstates [36].

Therefore, the total persistent current can be written as:

$$I_T = \sum_{n=1}^{N_e} I_n \qquad (2-22)$$

2-5 Drude weight

The Drude weight is the second derivative of ground-state energy, which given by [6]:

$$D = \frac{N}{4\pi^2}\frac{\partial^2 E}{\partial \Phi^2} \qquad (2-23)$$

where $N = N_{up} + N_{lo}$ gives total number of atomic sites in DMR. By using the dispersion relation in Eq. (2-15), the Drude weight can be written as,

$$D = \frac{N}{4\pi^2}\frac{1}{2}\left[\left(B_{up} + B_{lo}\right) - \frac{(A-B)\left(B_{up} - B_{lo}\right) + \left(X_{up} - X_{lo}\right)^2}{\sqrt{(A-B)^2 + 4V^2}} + \frac{(A-B)^2\left(X_{up} - X_{lo}\right)^2}{((A-B)^2 + 4V^2)^{\frac{3}{2}}}\right] \quad (2-24)$$

where,

$$B_{up} = \frac{8\pi^2}{N^2} t_{up} \cos\frac{2\pi}{N}\left(n + \frac{\Phi_{up}}{\Phi_0} + \frac{1}{2}\frac{\Phi_t}{\Phi_0}\right) \quad (2-25)$$

$$B_{lo} = \frac{8\pi^2}{N^2} t_{lo} \cos\frac{2\pi}{N}\left(n + \frac{\Phi_{lo}}{\Phi_0} - \frac{1}{2}\frac{\Phi_{lo}}{\Phi_0}\right) \quad (2-26)$$

2-6 Low-field magnetic susceptibility

The magnetic susceptibility at magnetic flux is given by [35]:

$$\chi(\Phi) = \frac{N^3}{16\pi^2}\frac{\partial I(\Phi)}{\partial \Phi} \quad (2-27)$$

we can be able to predict that the current is paramagnetic or diamagnetic in nature by depending on the sign of $\chi(\Phi)$. Here $\chi(\Phi)$ will determined only in the limit $\chi(\Phi) \rightarrow 0$ because we concerned to study the magnetic response in the low-field limit [9]. By using the persistent current in Eq. (2-19), the magnetic susceptibility can be written as,

$$\chi(\Phi) = \frac{N^3}{32\pi^2}\left[\left(B_{up} + B_{lo}\right) + \frac{(A-B)^2\left(X_{up} - X_{lo}\right)^2}{((A-B)^2 + 4V^2)^{\frac{3}{2}}} - \frac{\left((A-B)\left(B_{up} - B_{lo}\right) + \left(X_{up} - X_{lo}\right)^2\right)}{\sqrt{(A-B)^2 + 4V^2}}\right] \qquad (2-28)$$

Chapter Three

Results and Discussions

3-1 Energy spectrum in absence transverse magnetic flux

All energies and coupling strengths between subsystems were measured in units of $t_{lo} = 1\ eV$ where $c = e = h = 1$. All calculations achieved for no interacting systems of electrons. The energy spectrum of a double mesoscopic ring plotted as a function of magnetic flux in Figs. (3-1)-(3-4) for different factors in absence of transverse magnetic flux at zero temperature. The energies of the atomic sites were $E_{lo} = -E_{up} = 1$, the nearest neighbor hopping strength is $t_{lo} = t_{up} = 1$, the number of atoms in each ring are selected N=10 and N=20 as shown in Fig. (3-1a) and (3-1b), respectively. The parabola behavior of the energy levels as functions of the magnetic flux is still retained. The energy bands are symmetric in magnetic flux, due to the eigenenergies of double mesoscopic ring are symmetric in the wavevector. Energy levels in energy spectrum have maximum or minimum values with depends on the value of magnetic flux either half-integer or integer.

In Fig. (3-2), the energy spectrum as a function of magnetic flux presented for several values of $E_{lo} = 0.5,1,1.5,2$. The upper and lower energy bands shifted to the top and down, respectively. The upper energy band shifted by 0.4, while the lower energy band moves into down by 0.07. This means that changing the on-site energy E_{lo} greatly affects the upper energy band while its effect is slight on the lower energy band. This behavior reverses when E_{lo} is constant and E_{up} is changed.

While in Fig. (3-3), the range of the overlap zone obviously reduced as t_{up} decreased because bandwidth becomes narrow when t_{up} decreased. Noteworthy, energy spectrum shows that two different bands of energy levels appear, and they are separated by a finite energy gap. This energy gap is controllable by the two parameters. The first, energy gap decreases when nearest-neighbor hopping strength t_{up} increases due to increasing the probability of hopping the electron from an atomic site to nearest neighbor with the same ring. The second, the increment of inter-ring coupling lead to increasing of energy gap which depends on magnitude of inter-ring coupling, as illustrated in Fig. (3-4). To obviously understand the effect of inter-ring coupling strength on the behavior of the energy spectrum, it is presented in Fig. (3-4) for several values $= 0.5, 1, 1.5$ and 2. The two energy bands symmetrically shifted into the top and down, but the magnitude of shift increases as follows 0.3, 0.4 and 0.45, when inter-ring coupling strength increases as follows $1, 1.5$ and 2.

3-2 Persistent current

The persistent current measured in units t_{lo}. The current-flux characterizations for a double mesoscopic ring are shown in Figs. (3-5)-(3-8). The size of the ring is N=10 with the number of electrons $N_e =$ 6,7,8, and 9 in all Figs. (3-5)-(3-7). Both for the cases of even and odd N_e, the persistent current behaves as saw-tooth with sharp jumps at integer or half-integer multiples of flux- quantum Φ_0, respectively. These currents are periodic in magnetic flux. From the energy spectrum Fig. (3-1a), we see that at integer or half-integer multiples of flux-quantum, energy levels have either a maximum or a minimum value and it gives vanishing behavior of

persistent current at these specific values of Φ, since the current is obtained by taking the first order derivative of energy E(Φ) with respect to magnetic flux Φ. The amplitudes of the current clearly increase when the on-site energies increase. The amplitude of persistent current become 3, 2.4, 1.7, 0.9 at E=0.8 for the number of electrons $N_e = 6,7,8 \text{ and } 9$, respectively, as shown in Fig. (3-5). The effect t_{up} on the amplitude of persistent current is presented in Fig. (3-6). The amplitude of current at $t_{up} = 0.8$ is up to 2.65, 2.25, 1.6 and 1.1 for the number of electrons $N_e = 6,7,8 \text{ and } 9$, respectively. In Fig. (3-7), the persistent current plotted for several values of inter-ring coupling strengths. The amplitude of persistent current at V= 0.8 is 2.5, 2.1, 1.5, 0.8 for the number of electrons $N_e = 6,7,8 \text{ and } 9$, respectively.

The next observation is study persistent current in non-half-filling case and half-filling case for several values of $N_e = 6,16,26$, and $N_e = 7,17,27$ with ring size $N_{lo} = N_{up} = 26$ and $N_{lo} = N_{up} = 27$ as indicated in Figs. (3-8a) and (3-8b), respectively. Both results indicate that the amplitude of persistent current increases when the number of electrons increase. The electrons hop to the nearest neighbor sites depending on three important factors t_{up}, V, and E. All these factors enhance electron hopping, which leads to conducting phase in non-half-filling case. While electron hopping reduces as these factors decreases. The half-filling case can be clearly observed at $N_e = 26$ and $N_e = 27$. The persistent current is completely vanishes at $N_e = 26$ and $N_e = 27$ for even and odd number of electrons, in half-filling case ($N_{lo} = N_{up} = 26$ and $N_{lo} = N_{up} = 27$), respectively. This case exhibit an insulating phase. The vanishing behavior of current can be understood as followed. The probability of hopping the electron to the

neighboring sites will disappear because most atomic sites are occupied with electrons in half-filling case. Also notice that there is an additional reduction gets to the current when increasing the number of electrons by the proportion of the number of atoms when the number of electrons almost to half-filling case, the current will be reduced because of the probability of hopping the electron to the neighboring sites will decrease as a result of most atomic sites are occupied with electrons.

In order to understand behavior of persistent current in double mesoscopic ring consist of the same type of atomic sites or two different types of atomic sites, the result presented in Fig. (3-9). At similar values of on-site energies $E_{lo} = E_{up} = E = 0.8$, the amplitude of persistent current is about 3.4 for even number of electrons, while it becomes 2.7 for odd number of electrons as shown in Figs. (3-9a) and (3-9b), respectively. At dissimilar values of on-site energies $E_{lo} = -E_{up} = E = 0.8$, the amplitude of persistent current decreases to 3 and 2.4 for even and odd number of electrons as indicated in Figs. (3-9c) and (3-9d), respectively.

In Fig. (3-10) we present the variation of I_{max} with ring size N taking the maximum absolute value of current amplitude of the current-flux curve. With these dots we establish a scaling relation of the form: $I_{max} = DN^{-\alpha}$. In order to investigate the asymptotic behavior of persistent current as a function of ring size. Where the exponent α becomes 1.495 in case odd and 1.053 in case even. Whereas the factor D depends on system size where D=81.629 and D=30.357 for the odd and even number of electrons, respectively. These curves show that current decays algebraically by increasing system size.

3-3 Drude weight

The Drude weight as a function of the number of atomic sites N presented in Figs. (3-11)-(3-13) in order to study the nature of conducting of the considered system. when the number of electron $N_e = 10$, observe increase in Drude weight compare with decrease N.

All the results of the Drude weight calculated at N=4n+2. The Drude weight clearly vanishes at large sizes of double mesoscopic rings. In Fig. (3-11), the Drude weight plotted for many values of on-site energies $E_{lo} = -E_{up} = 0.2,0.4,0.6,0.8$. At small sizes of double mesoscopic ring, the Drude weight increases when on-site energy decreases, which reaches to 1.65 at $E = 0.2$. In addition to, the Drude weight vanishes at N=20. While, the Drude weight increases as inter-ring coupling strength increases, where reaching to 1.25 at V=0.8, as shown in Fig. (3-12).

The Drude weight curves for several values of $t_{up} = 0.2,0.4,0.6,0.8$, are becoming more distinct than previous cases. However, the curves at t_{up} small are vanish faster than that at t_{up} large, as indicated in Fig. (3-13) the vanishing behavior of Drude weight shows the crossing of the system from the conducting phase to the insulating phase.

3 -4 Low-field magnetic susceptibility

The current can be controlled whether is diamagnetic or paramagnetic by calculating low-field magnetic susceptibility at $\Phi \to 0$. In Fig. (3-14), the total magnetic susceptibility with the quantum number n, which lies in the range $\frac{-N_e}{2} < n < \frac{N_e}{2}$, plotted as a function of N_e , where N_e represents the

number of electrons. The low-filed magnetic susceptibility have diamagnetic behavior at $\Phi \to 0$, which means only diamagnetic persistent current in the double mesoscoping ring. To understand this behavior will compare the Fig. (3-14) with Fig. (3-5a) and (3-5b), at $\Phi = 0$. The persistent current has a negative slope at $\Phi = 0$, which means diamagnetic persistent current.

Now, we discuss the variation of low-field magnetic susceptibility with system size N for double mesoscopic ring in the half-filled case. Figs. (3-15a) and (3-15b) correspond to the change of low-field magnetic susceptibility for even and odd number of atomic sites N = 4n+2 and N=4n+1, respectively. It is observed that both for even and odd N, low-field current exhibits diamagnetic nature. Thus, in brief, we say that for non-interacting half-filled rings low-field current exhibits diamagnetic response irrespective of N i.e., whether N is even or odd.

3-5 Energy spectrum with presence transverse magnetic flux

Now, the results with presence transverse magnetic flux are presented. Firstly the double mesoscopic ring with one type of atoms is considered. The inter-ring coupling strength opens gap between the upper and lower bands with magnitude 2V, thus avoiding intersections at $\Phi = 0$, as presented in Fig. (3-16a). The magnitude of energy gap is not affected by the transverse flu, as shown in Fig. (3-16b) and (3-16c) at $\Phi_t = 2$ and 3, respectively.

In Fig. (3-17) the bottom of lower band for several values of transverse flux$\Phi_t = 1,2,3$ located at the values of AB flux$|\Phi = 0.5,1,1.5|$, respectively. This means that the transverse flux controls the values of

allowed quasimoment by magnitude $\frac{\Phi_t}{2}$ from through relation $\left(q = \frac{2\pi}{N}(n + \frac{\Phi}{\Phi_0} + \frac{1}{2}\frac{\Phi_t}{\Phi_0})\right)$.

The energy spectrum of ground state (n=0) for two different types of atoms ($E_{lo} = -E_{up} = 1$) is indicated in Fig. (3-18). The energy spectrum, non-monotonously behaves. The upper and lower band do not crossing in case $\Phi_t = 1$ on all rang Φ, but in case $\Phi_t > 1$ note cross two bands at certain value of Φ depending on the transverse flux value. At $\Phi_t = 2$, the energy bands cross at $\Phi = 1.6$ and 3.4, while the range of crossing increases of value $\Phi_t = 3$ at $\Phi = 1$ and 4. These intersections repeated in periodic by magnitude $\Phi = 10$.

The PC greatly affected by the transverse flux as shown in Fig. (3-19) at $E_{lo} = E_{up} = 1$ and V=0.2 for several values of $\Phi_t = 1,2,3,4$. The curvature of PC will increase by increasing Φ_t. In addition to, the amplitude of persistent current is increase by increasing transverse flux.

In Fig. (3-20) the amplitude of persistent current is asymmetry around zero in case $E_{lo} = -E_{up} = 1$, when the transverse flux $\Phi_t = 1$, as shown Figs. (3-20a) and (3-20b) while in case $\Phi_t = 2$, the asymmetry will increase, as shown in Figs. (3-20c) and (3-20d). The periodicity of persistent current is shifted by order 0.5 into negative scale, this mean from -1.5 to 0.5. This characteristic can be understand from non-monotonus behavior of energy spectrum in Fig. (3-19).

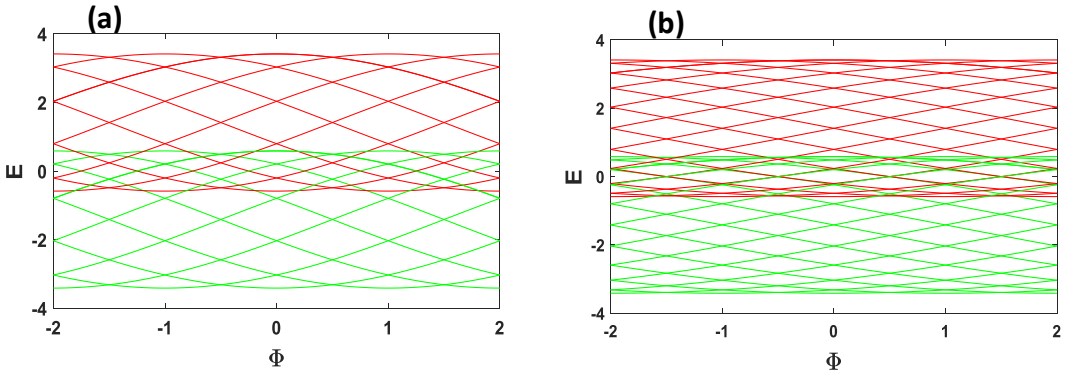


Fig. (3-1): Energy spectrum of mesoscopic ring with $E_{lo} = -E_{up} = 1, t_{lo} = t_{up} = 1$, $V = 1$, the number of sites (a) N=10, (b) N=20.

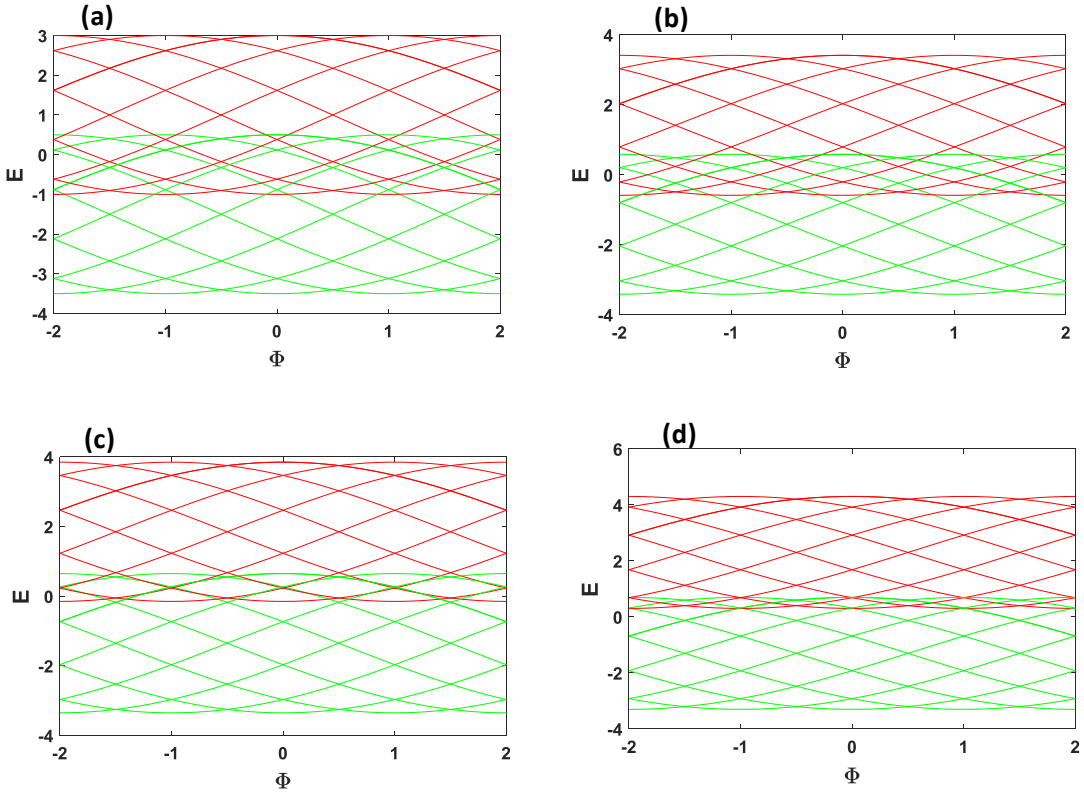


Fig. (3-2): Energy spectrum of mesoscopic ring with $t_{up} = 1$, $E_{up} = -1, V = 1$, and the number of atomic sites N=10 (a) $E_{lo} = 0.5$, (b) $E_{lo} = 1$, (c) $E_{lo} = 1.5$, (d) $E_{lo} = 2$.

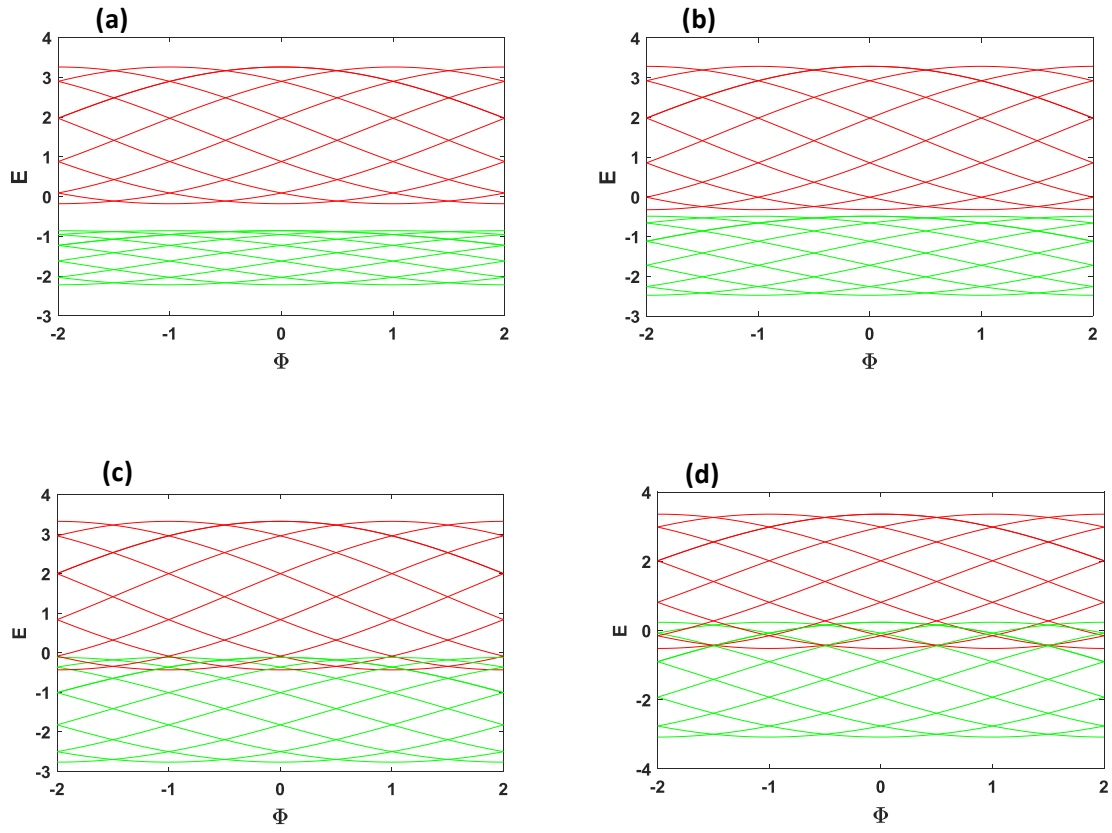


Fig. (3-3): Energy spectrum of mesoscopic ring with $t_{lo} = 1$, $E_{up} = -1, V = 1$, and the number of atomic sites N=10 (a) $t_{up} = 0.2$, (b) $t_{up} = 0.4$, (c) $t_{up} = 0.6$, $t_{up} = 0.8$.

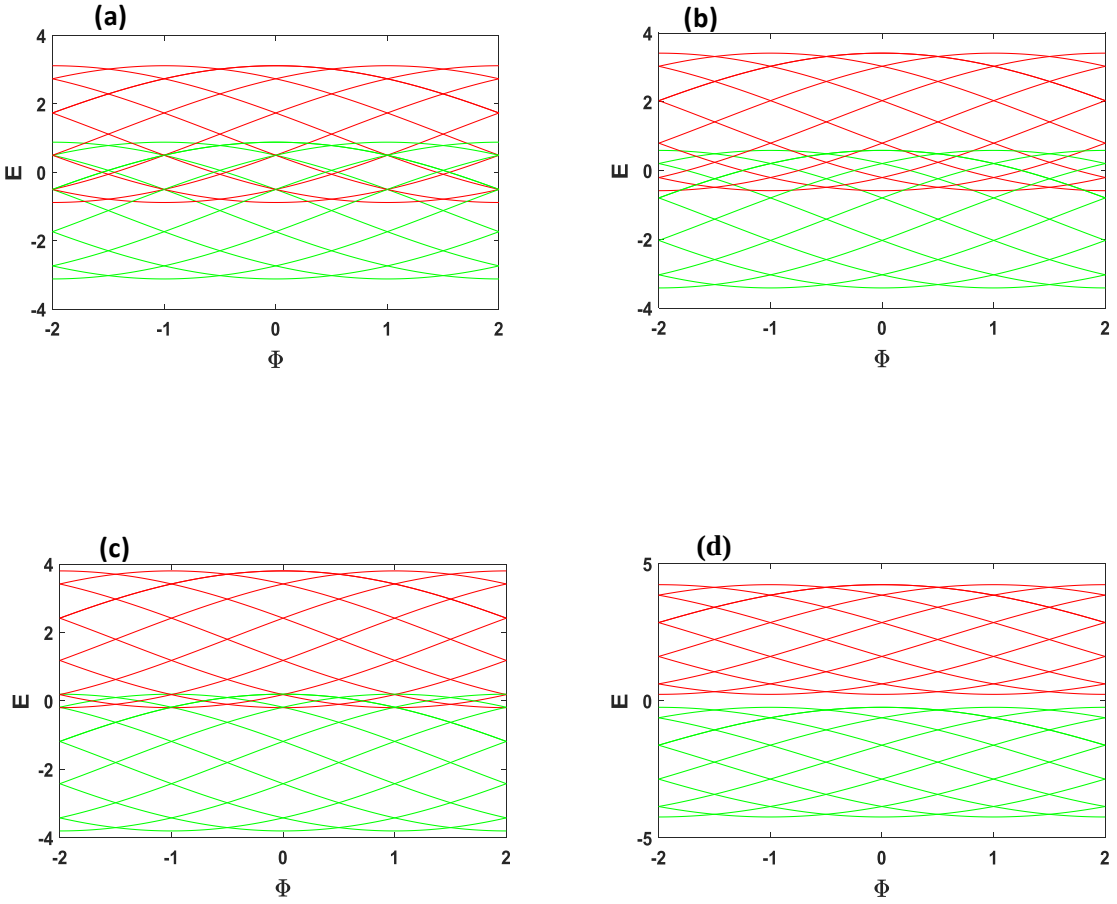


Fig.(3-4): Energy spectrum of mesoscopic ring with $t_{lo} = t_{up} = 1$, $E_{lo} = -E_{up} = 1$, and the number of atomic sites N=10 (a) $V = 0.5$, (b) $V = 1$, (c) $V = 1.5$, (d) $V = 2$.

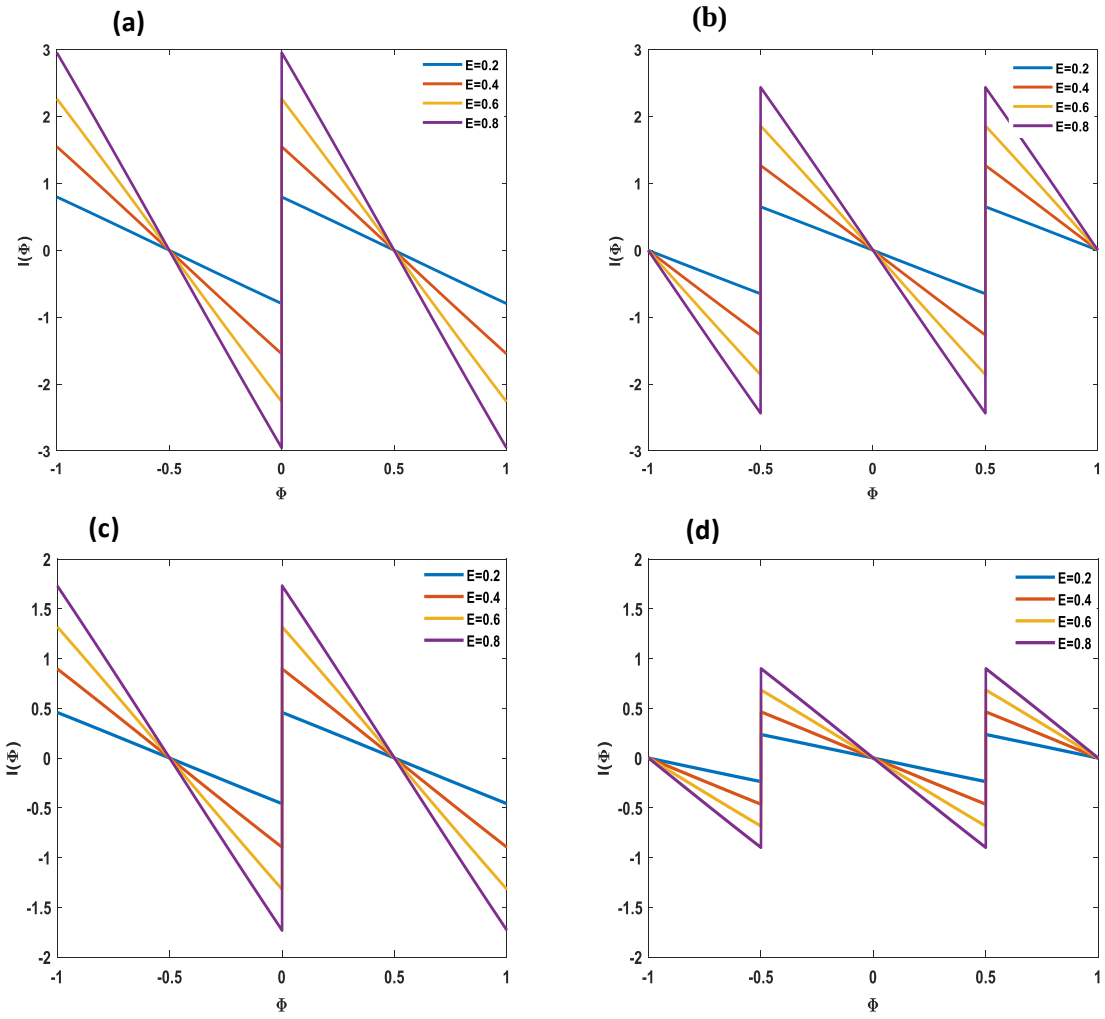


Fig. (3-5): Persistent current as a function of magnetic flux with N=10, $t_{lo} = 1, t_{up} = 0.5$, $V = 1$, for several values of atomic sites $E_{lo} = -E_{up} = 0.2, 0.4, 0.6, 0.8$. The number of electrons are (a) $N_e = 6$ and (b) $N_e = 7$ (c) $N_e = 8$ (d) $N_e = 9$.

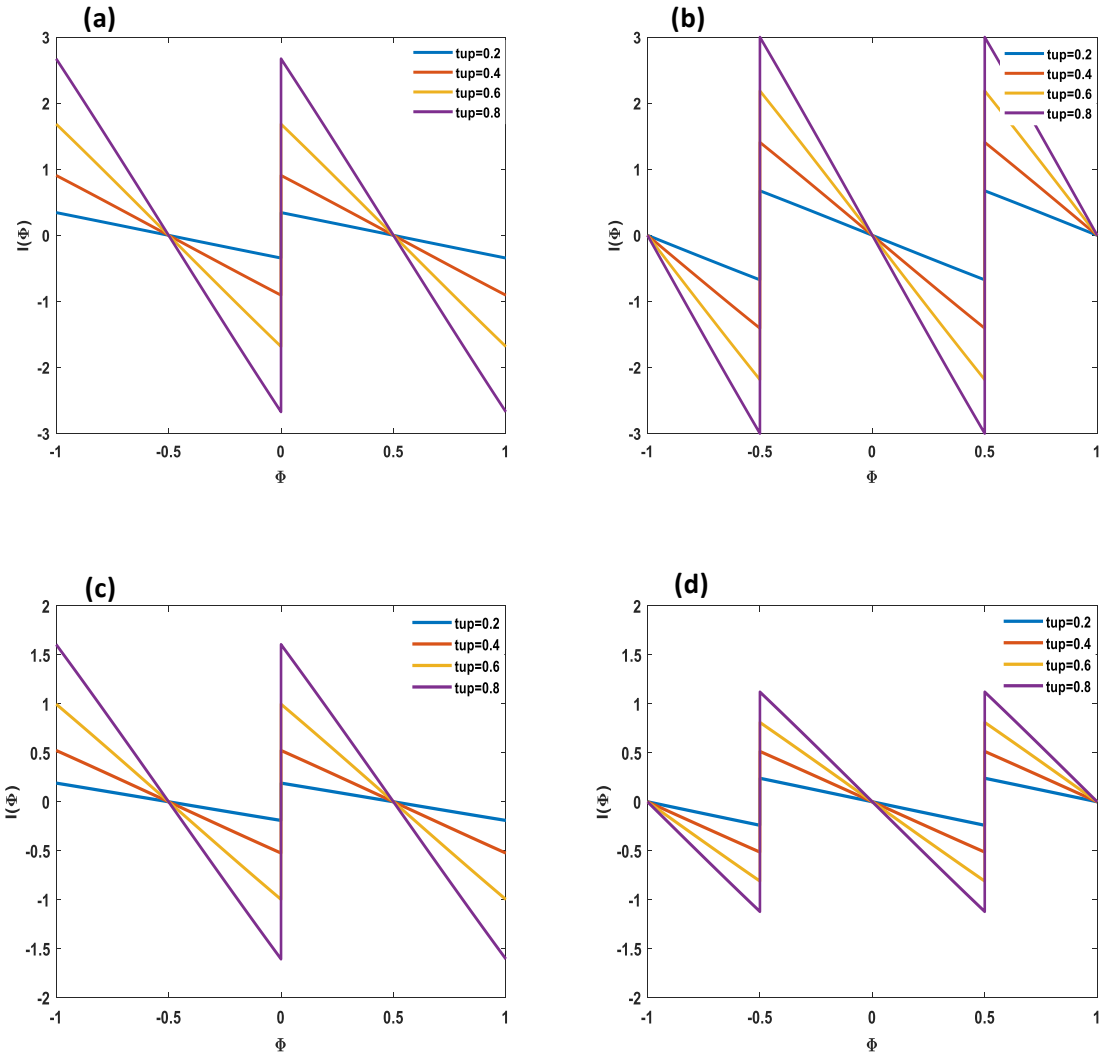


Fig. (3-6): Persistent current as a function of magnetic flux with N=10, $E_{lo} = -E_{up} = 1, t_{lo} = 1, V = 1$, for several values of atomic sites $t_{up} = 0.2, 0.4, 0.6, 0.8$. The number of electrons are (a) $N_e = 6$ and (b)$N_e = 7$ (c) $N_e = 8$ (d) $N_e = 9$.

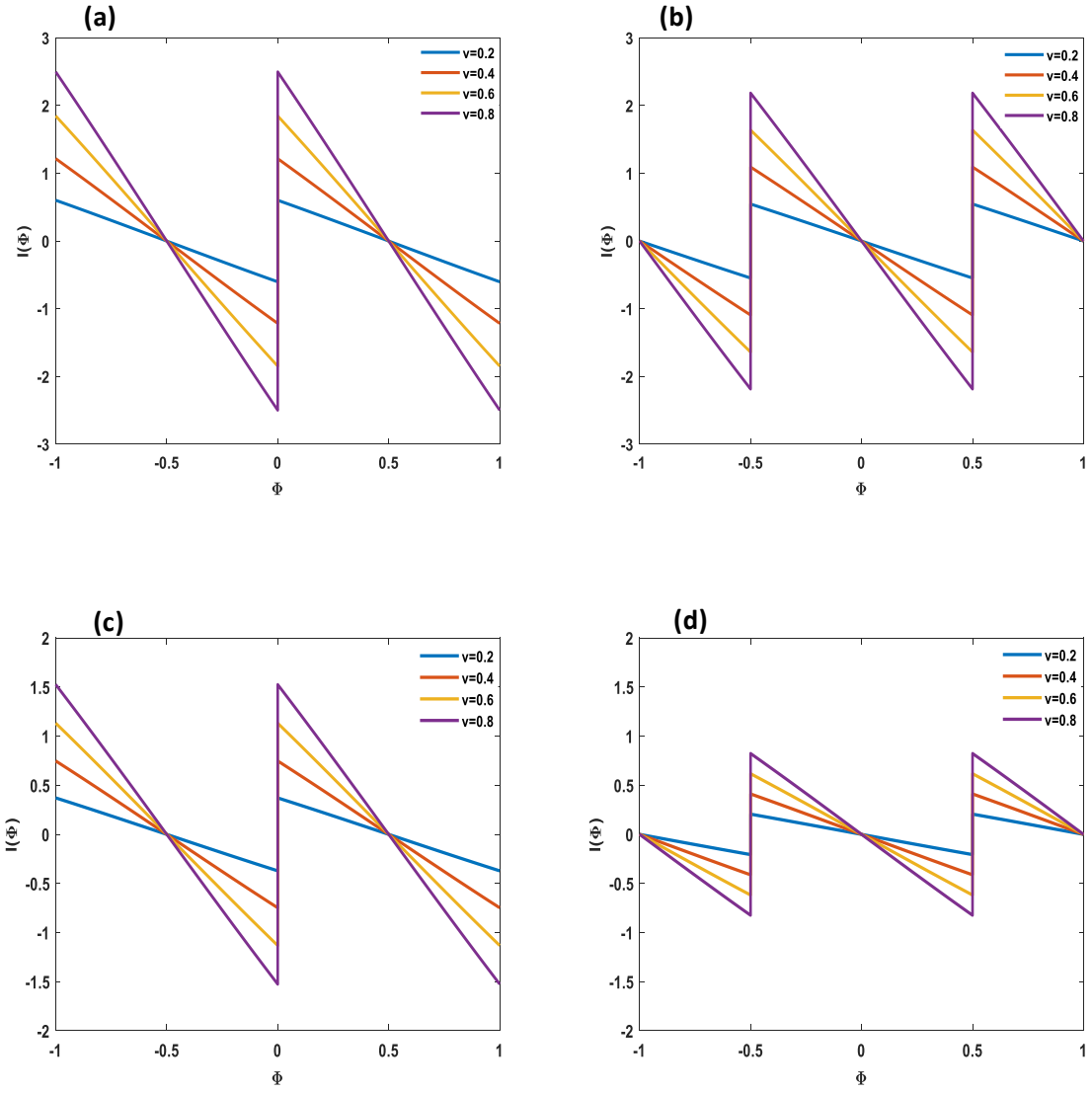


Fig. (3-7): Persistent current as a function of magnetic flux with N=10, $E_{lo} = -E_{up} = 1$, $t_{lo} = 1, t_{up} = 0.5$, for several values of atomic site $V = 0.2, 0.4, 0.6, 0.8$. The number of electrons are (a) $N_e = 6$ and (b)$N_e = 7$ (c) $N_e = 8$ (d) $N_e = 9$.

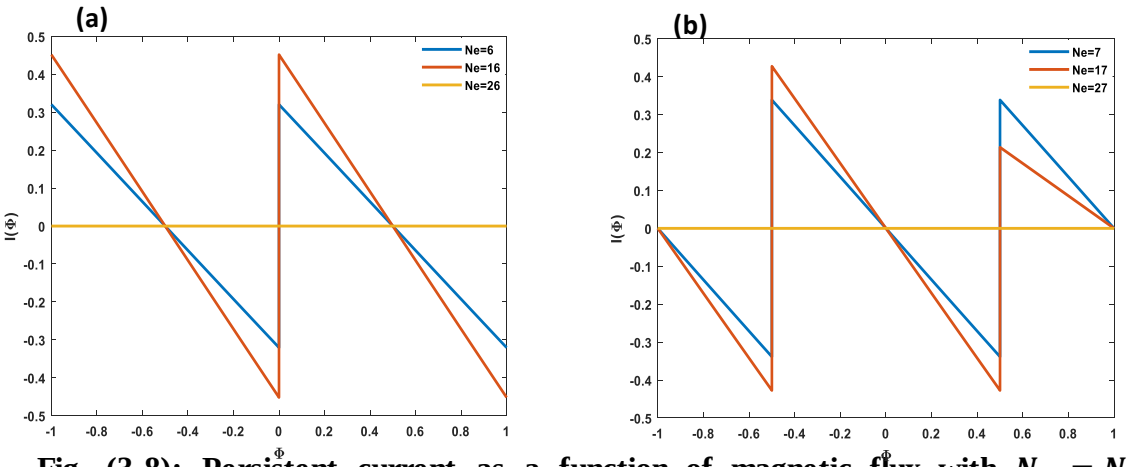


Fig. (3-8): Persistent current as a function of magnetic flux with $N_{lo} = N_{up} =$ 26 and 27, $E_{lo} = -E_{up} = 1$, $t_{lo} = t_{up} = 1$, V = 1.The number of electrons are (a) even $N_e = 6, 16, 26$ and (b) odd$N_e = 7, 17, 27$.

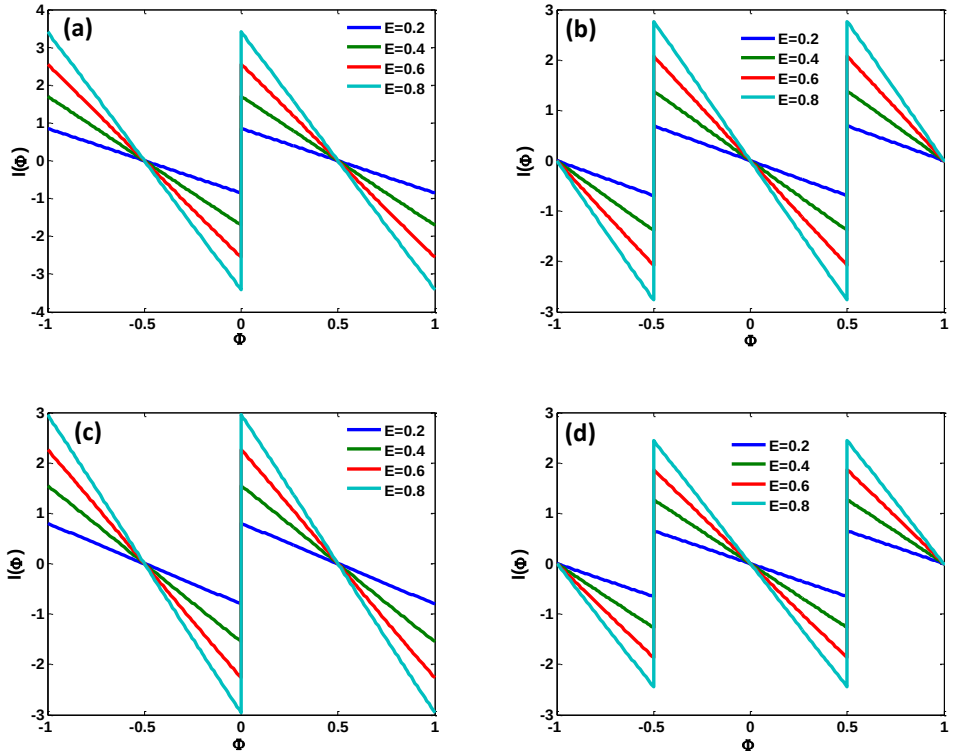


Fig. (3-9): Persistent current as a function of magnetic flux with N=10, $t_{lo} = 1, t_{up} = 0.5$, $V = 1$, for similar values of on-site energies $E_{lo} = E_{up} = E = 0.2, 0.4, 0.6, 0.8$ in (a) $N_e = 6$ and (b) $N_e = 7$. While dissimilar values of on-site energies $E_{lo} = -E_{up} = E = 0.2, 0.4, 0.6, 0.8$ in (c) $N_e = 6$ and (d) $N_e = 7$.

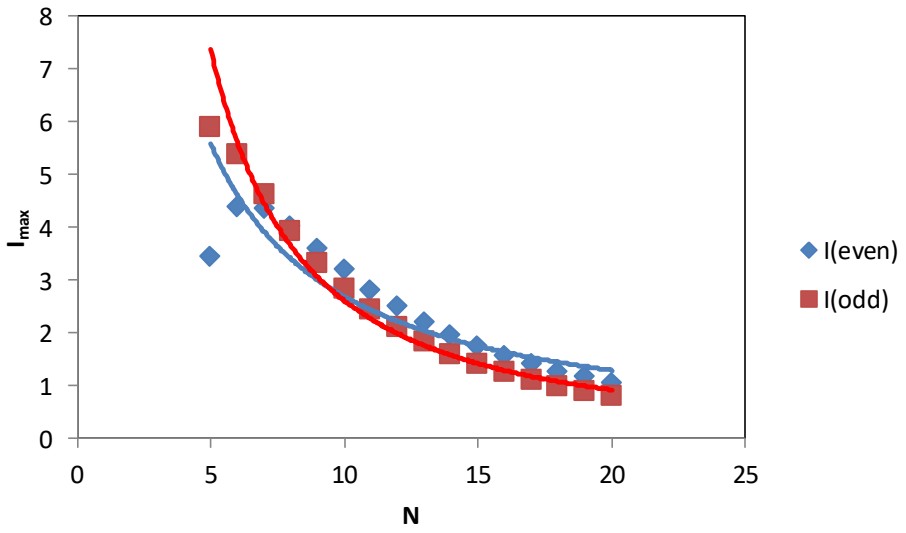


Fig. (3-10): Variation of persistent current with ring size N with $E_{lo} = -E_{up} = 1, V = 1, t_{lo} = t_{up} = 1$. Using these dots we find a scaling relation between the current and ring size which generates the blue line and red line for even and odd number of electrons. The even and odd number of electrons are analyzed depending on Ne=4and 3, respectively.

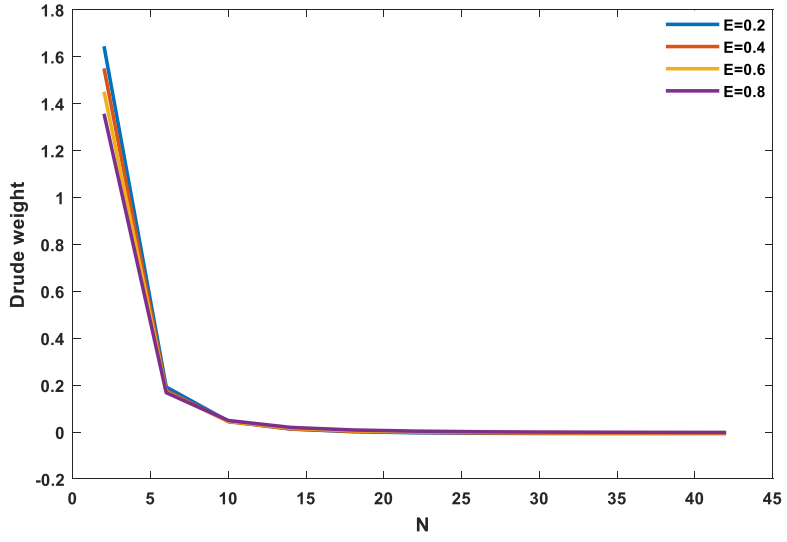


Fig. (3-11): Drude weight as a function of the ring size, $t_{lo} = 1, t_{up} = 0.5, V = 1$, $N_e = 10$, for several values of on-site energies $E_{lo} = -E_{up} = 0.2, 0.4, 0.6$ and 0.8.

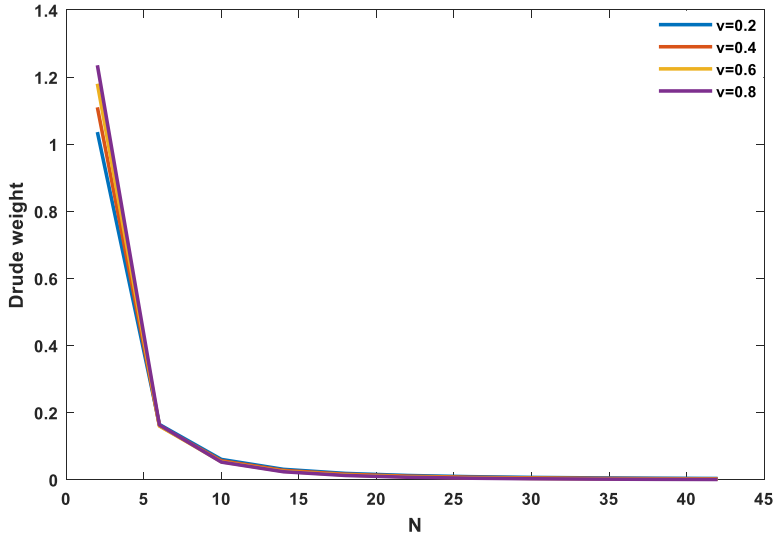


Fig. (3-12): Drude weight as a function of the ring size, $t_{lo} = 1, t_{up} = 0.5$, $E_{lo} = -E_{up} = 1$, for several values of atomic sites$V = 0.2, 0.4, 0.6, 0.8$. The number of electrons are $N_e = 10$.

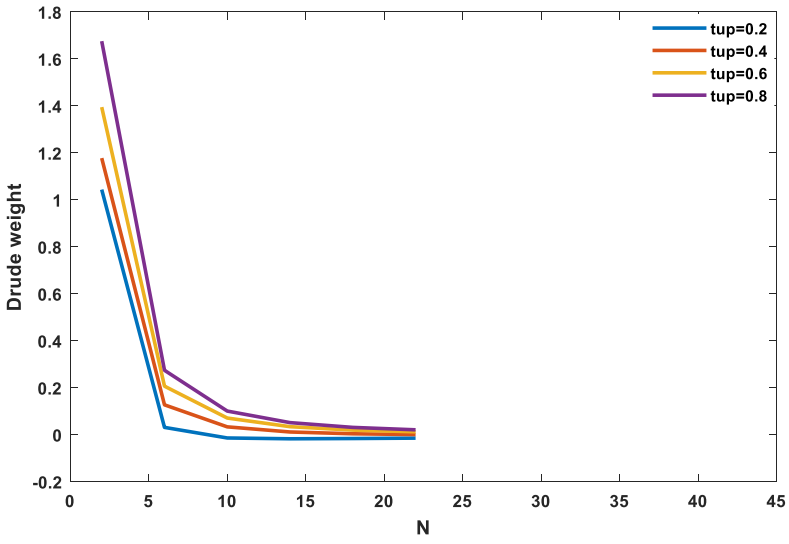


Fig. (3-13): Drude wieght as a function of the number of atomic sites, $E_{lo} = -E_{up} = 1$, V=1, $t_{lo} = 1$, for several values of atomic sites $t_{up} = 0.2, 0.4, 0.6, 0.8$. The number of electrons are $N_e = 10$.

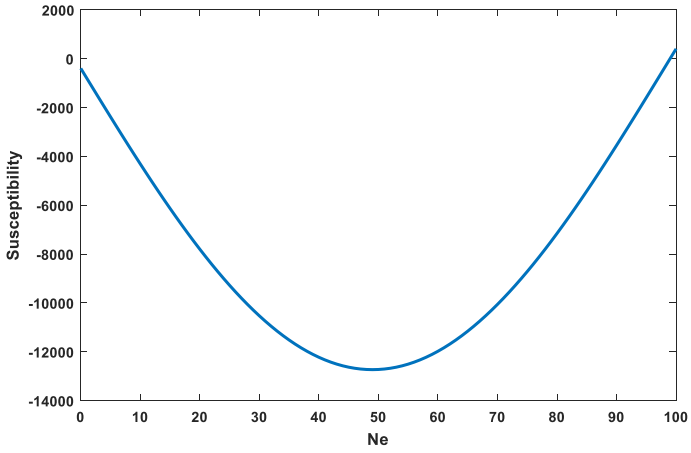


Fig. (3-14): Low-field magnetic susceptibility as a function of the number of electrons N_e , $E_{lo} = -E_{up} = 1$, V = 1, $t_{lo} = t_{up} = 1$.

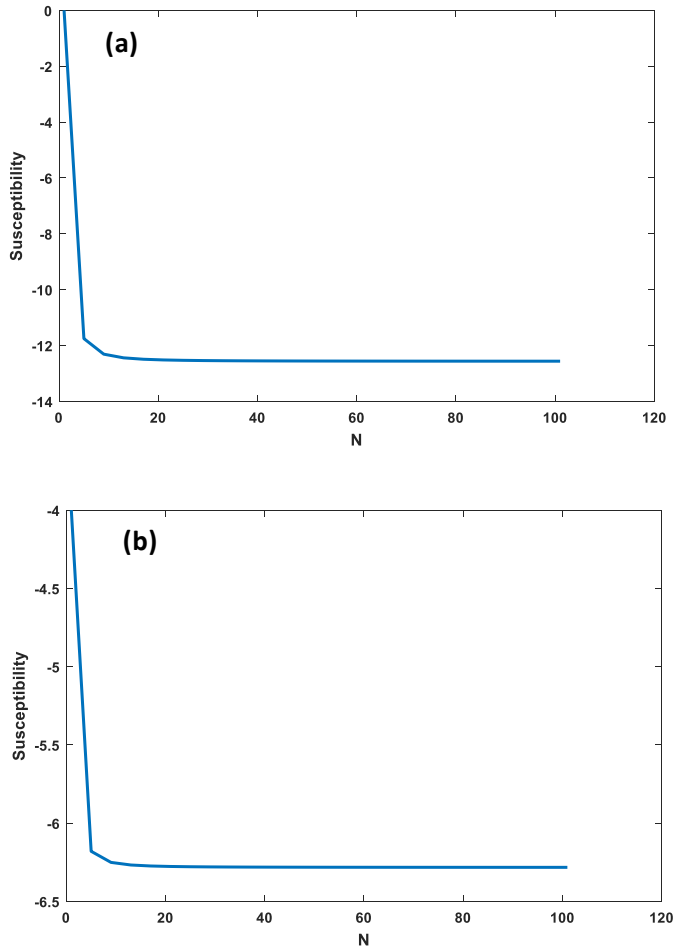


Fig. (3-15): Low-field magnetic susceptibility as a function of the number of atomic sites (a) N=4n+2, (b) N=4n+1, $E_{lo} = -E_{up} = 1$, V = 1, $t_{lo} = t_{up} = 1$, $N_e = 25$.

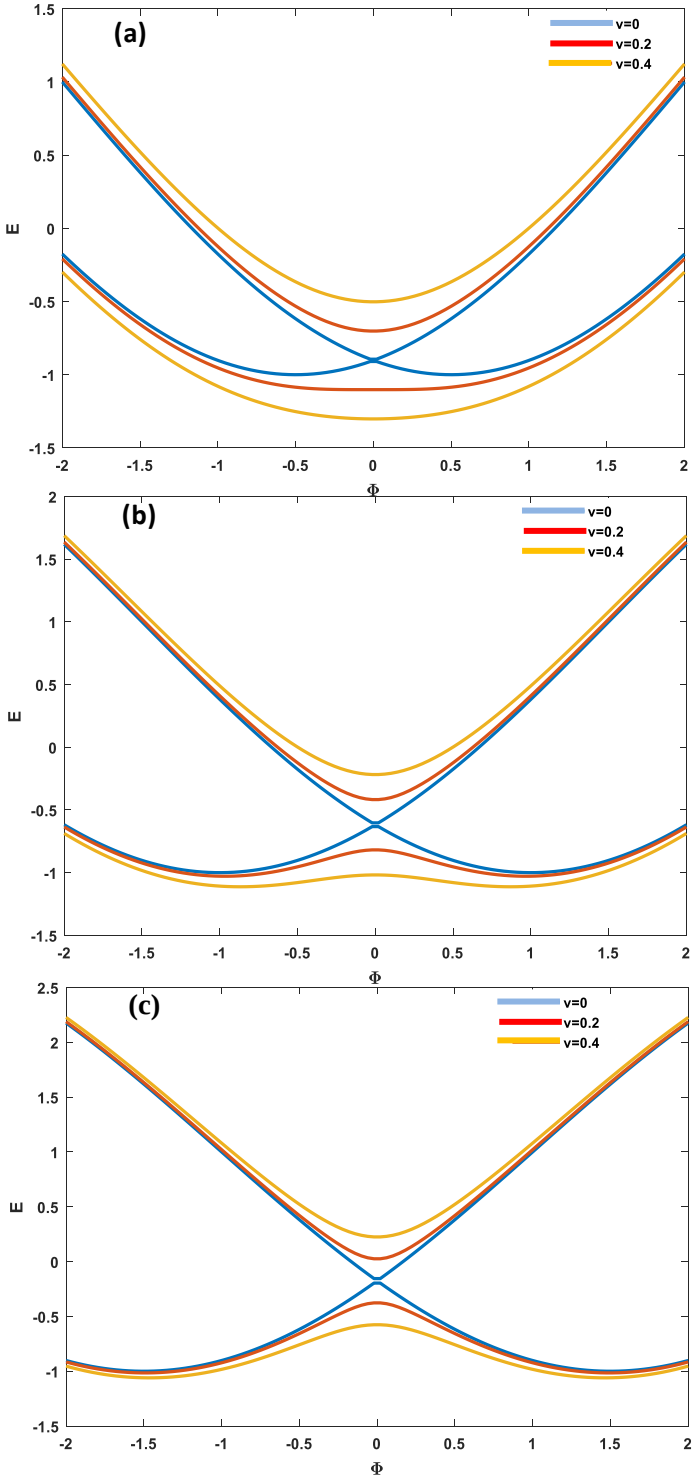


Fig. (3-16) Energy spectrum for ground state (n=0) at $t_{up} = t_{lo} = 1$, $E_{lo} = E_{up} = 1, V = 0, 0.2, 0.4$ at $\Phi_t = 1$, $\Phi_t = 2, \Phi_t = 3$.

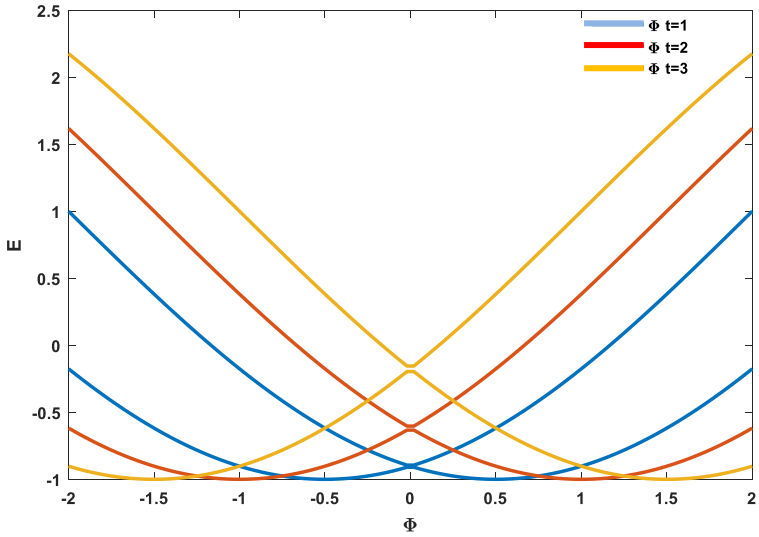


Fig. (3-17) Energy spectrum for ground state (n=0) at $t_{up} = t_{lo} = 1$, $E_{lo} = E_{up} = 1, V = 0$ at $\Phi_t = 1, 2, 3$.

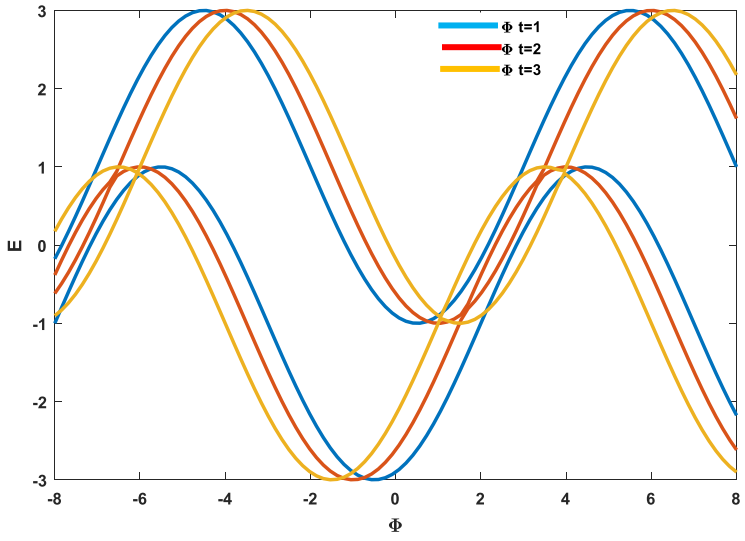


Fig. (3-18): Energy spectrum for ground state (n=0) at $t_{up} = t_{lo} = 1$, $E_{lo} = -E_{up} = 1$, V = 0 at $\Phi_t = 1, 2, 3$.

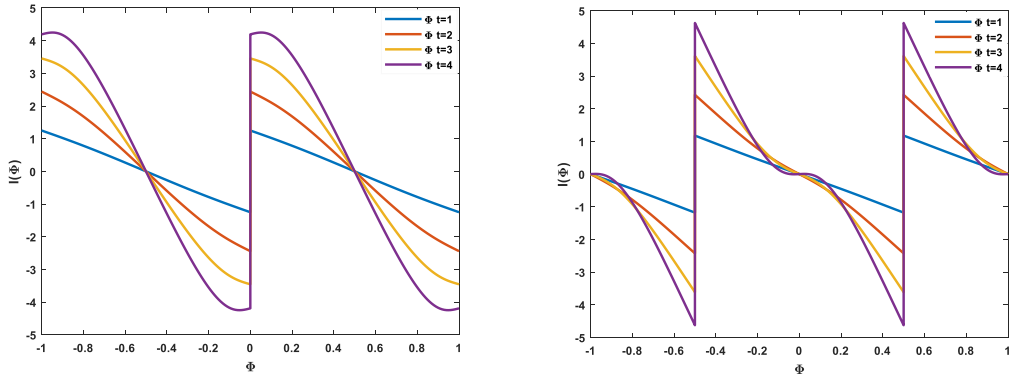
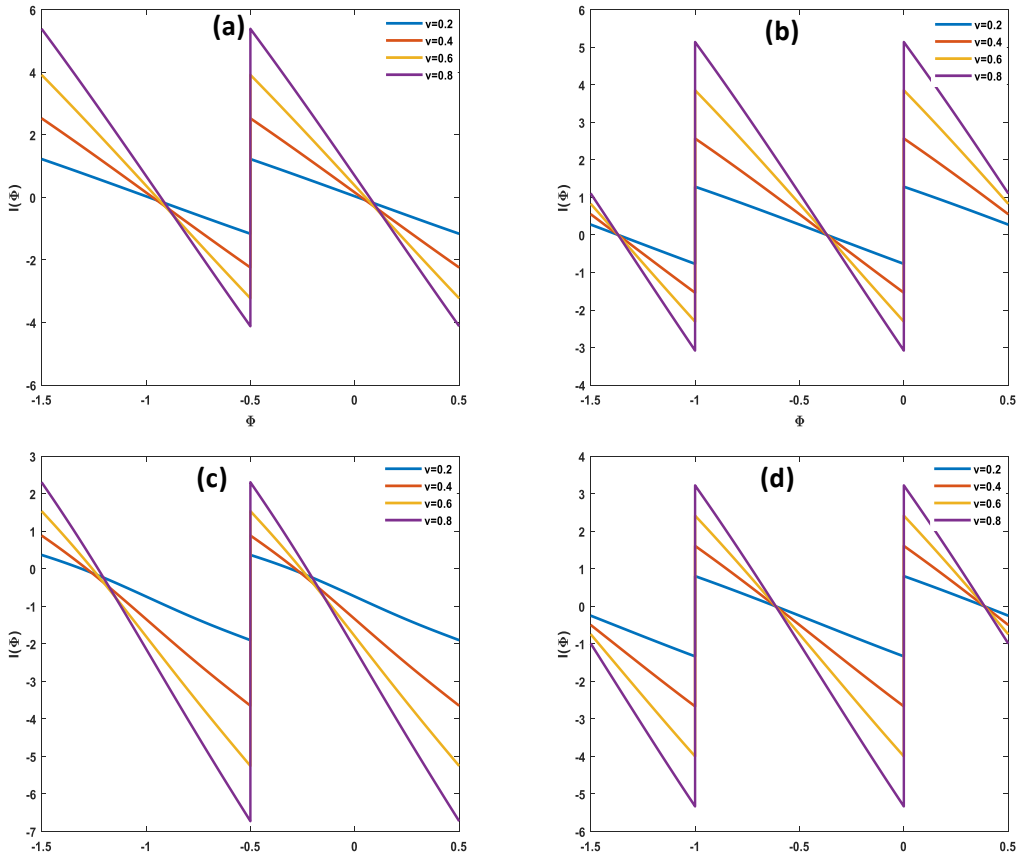


Fig. (3-19): Persistent current as a function of magnetic flux with N=10, $E_{lo} = E_{up} = 1$, $t_{lo} = 1, t_{up} = 1, V = 0.2$, For several values of transverse flux $\Phi_t = 1, 2, 3, 4$. The number of electrons are (a) $N_e = 6$ and (b) $N_e = 7$.



-Fig. (3-20): Persistent current as a function of magnetic flux with N=10, $E_{lo} = -E_{up} = 1$, $t_{lo} = 1, t_{up} = 1, V = 1$, For several values of transverse flux (a) and (b) $\Phi_t = 1$, (c) and (d) $\Phi_t = 2$. The number of electrons are (a) and (c) $N_e = 6$, (b) and (d) $N_e = 7$.

Chapter Four

Density Functional Theory Calculations

4-1 Introduction

A proper understanding of the electronic properties of nanostructures is crucial for several domains of progress nanotechnology. Metal rings with thickness in few nanometer range, possesses unusual chemical and physical properties, because of quantum confinement and surface effects[46].

These structures exhibit a quantized conductance and have unique structural properties. It is known that the properties of metal nanostructures are closely related to their crystal structure. Noble metals exhibit various crystal structures in the bulk for despite promising applications of noble metal nanoplates, nanosheets and nanowire, their use is fixed due to their high costs and scarce reserves[47].

Mixing noble metals with minerals that are abundant in the earth can improve their properties [48]. Note that the heterogeneous Ag-Au[49], Ag-Cu[50] and Au-Cu[51] nanostructures with much better properties than their clean counterparts have been manufactured for wide applications in several fields like opticoelectronics, protective coatings, electronics, drug delivery, bio-sensing and catalysis.

Here, the results presented of a DFT study of the electronic properties of several ring structures such as single metallic ring (with 3, 4, 5 and 6 atoms), pristine double metallic ring and alloyed double metallic ring. Pristine double metal ring consists of two metal rings with the same type of metal, while alloyed double metal ring consists of two metal rings with two different types of metals. The used metals are Au, Ag and Cu.

4-2 Computational Details

All quantum calculations were achieved with standard Gaussian 09W software package [52] with DFT to calculate the basic properties of the metal rings under study in their ground electronic states. Thus, all the parameters presented in this study: the optimized geometry, highest occupied molecular orbital (HOMO), lowest unoccupied molecular orbital (LUMO), energy gap, chemical hardness, electronegativity and chemical softness were calculated at the hybrid functional B3LYP, which combines Beckes exchange and Lee *et al.* correlation functional with LanL2DZ basis set [53].

The LanL2DZ besis set is the Los Alamos National Laboratory besis set, which developed by Hay and Wadt [54, 55]. This besis set used in the study of compounds or clusters containing heavy elements [56, 57]. The electronegativity which is describes the escaping tendency of electrons from the system. Let E(N) be a ground-state electronic energy as a function of the number of electrons N . As is well-known, the derivative as a function of N at a constant external potential $V(\vec{r})$ is the chemical potential or the negative of the absolute electronegativity, where [58, 59].

$$\mu \approx \left(\frac{\partial E}{\partial N}\right)_{V(\vec{r})} \approx -\chi \qquad (4-1)$$

The theoretical definition of chemical hardness has been given by the DFT as the second derivative of electronic energy as a function of the number of electrons N at a constant external potential $V(\vec{r})$ [58, 60].

$$\eta = \frac{1}{2}\left(\frac{\partial^2 E}{\partial N^2}\right)_{V(\vec{r})} = \frac{1}{2}\left(\frac{\partial \mu}{\partial N}\right)_{V(\vec{r})} \qquad (4-2)$$

Chemical hardness is the resistance of the chemical potential to change in the number of electrons. Using a finite difference approximation, a working equation for the computation of chemical hardness and electronegativity can be written as [58, 60].

$$\chi = \frac{E_{HOMO}+E_{LUMO}}{2} \qquad (4-3)$$

$$\eta = \frac{E_{LUMO}-E_{HOMO}}{2} = \frac{E_g}{2} \qquad (4-4)$$

The chemical softness is a property of molecules that measures the extent of chemical reactivity. It is the reciprocal of chemical hardness [58, 60]

$$S = \frac{1}{2\eta} = \left(\frac{\partial^2 N}{\partial E^2}\right)_{V(\vec{r})} = \left(\frac{\partial N}{\partial \mu}\right)_{V(\vec{r})} \qquad (4-5)$$

Electrophilicity is a measure of energy reducing of the chemical samples due to maximum value of electron flow between donor and acceptor. Electrophilicity (ω) is defined as[58].

$$\omega = \frac{\chi^2}{2\eta} \qquad (4-6)$$

There are two different methods to calculate the above the global quantities, the first is a finite difference approximation which based on the differences of total electronic energies as an electron is added or removed in associated with the neutral molecule. The second is Koopman's theorem, which established on the differences between the HOMO and LUMO energies for the neutral molecule[61].

4-3 Computational Results

4-3-1 Equilibrium geometries

Before proceeding in physical properties calculation, it is necessary to find out the geometry optimization of the metal rings. The equilibrium geometries for

all studied systems were optimized at the DFT level of theory by using a B3LYP functional together with the standard LANL2DZ basis set in the gaseous phase and for a better approximation of the experimental parameters.

The optimized geometries, HOMO and LUMO shapes of single metal rings R_n where n indicate to nmber of atoms (n=3-5), while R refers to type of noble metal (R: Au, Cu and Ag), as shown in Figs. (4-1)-(4-3), respectively. Figs. (4-4) and (4-5) represent the optimized geometries, HOMO and LUMO shapes of pristent and alloyed double metal rings. As can be seen in all the pristine and alloyed metal rings, their DOS near the LUMO level has a distinct variation compared to that of the single metal ring, resulting in a reduction of the band gap and therefore an electrical conductivity increase. So the energy gap is a key factor to enhancement the electrical conductivity of a material, as shown in following relation [62, 63].

$$\sigma\alpha\ exp\left(-\frac{E_g}{2k_BT}\right) \qquad (4-7)$$

where, $\sigma, k_B,$ and T, are the conductivity, the Boltzmann's constant, and the temperature 298.14 K, respectively. Reducing the energy gap is an important in the application of metal rings because of the new systems have more reactive in charge transfer process and have good semiconductor properties to using as nanoelectronic devices. Since the DOS is accordance with the eigenenergies of the metal ring itself. The DOS is change due to varying the number of atoms and type of material.

4-3-2 Frontier Orbital Energies

To describe the chemical behavior of investigated systems, the frontier molecular orbital theory was employed. The energy of HOMO is already accordance with the ability to give the electron to the metal rings, whereas the

energy of LUMO is accordance with the ability to accept the electron from the metal rings.

Therefore, high value of HOMO energy refers to high desire to give electrons to appropriate acceptor molecule with low empty molecular orbital energy. Likewise, low value of LUMO energy refers to high desire to accept electrons from the metal surface. The energy gap between the HOMO and LUMO of the metal rings is another important character that should be studied. Large values of the energy gap mean high electronic stability and then low reactivity, but low values represent easily removing an electron from the HOMO orbital to LUMO, which can result in good reactivity [64, 65].

In order to clearly understand the changes of electronic properties, it is essential to calculate the DOS of the metal rings. Figs. (4-6)-(4-9) show the DOS analysis, which consists of the conduction and valence bands and the energy gap [51]. The energy gap between HOMO and LUMO indicates the chemical stability of molecules. As the number of atoms in the studied system is odd, which lead to the number of electrons is odd, that molecular orbital will split into alpha and beta molecular orbitals. This behaviour generates alpha and beta types for each of virtual, occupied orbitals and DOS spectrum, as explained in Figs. (4-6a), (4-6c), (4-7c), (4-7a), (4-8a) and (4-8c). It is noted that the DOS of HOMO orbitals increase by increasing of the number of atoms in metal ring for all nobel metals, due to the concentration of occupied orbitals in a narrow range of energy, while virtual orbitals are in a wide range of energy.

In order to gain a clear understanding of the electronic properties in metal rings, energy gaps are calculated. The energy gaps of each type of noble metals in the single metal rings are order as following $R_5 > R_6 > R_3 > R_4$ where (R: Au, Cu and Ag), as listed in Tables (4-1)-(4-3). The energy gaps of the pristine

double metal ring are ordered as following $2Cu_6 > 2Au_6 > 2Ag_6$(Table (4-4)), because the energy gaps of single metal ring follow the trend $Cu_6 > Au_6 > Ag_6$.

It is noted that the energy gaps of alloyed double metallic ring are within the range of its pristine counterparts. Amongst the alloyed double metal rings, Cu_6Au_6 has the highest energy gap that changes as $Cu_6Au_6 > Cu_6Ag_6 > Ag_6Au_6$. This trend is due to the large energy gap of Cu_6. Another important observation, R_5 system is more stable and less reactive because of energy gap is high. These values of the energy gap showing a semiconductor character.

4-3-3 Global Reactivity Descriptors

Depending on HOMO and LUMO values for the study systems, the global chemical reactivity descriptors, such as electronegativity, chemical softness, chemical hardness, and electrophilicity are listed in Table (4-1)-(4-5). The chemical softness and hardness are very important properties to determine the stability and reactivity of the molecules. Soft molecule is more reactive than hard molecule because it can easily donate electrons [66, 67] . Hence, the highest values of chemical softness for single metal rings are in order $Ag_4 > Cu_4 > Au_4$. While $2Ag_6$ obtained highest value of chemical softness with respect its alloyed counterpants. Table (4-1)-(4-3) presents the large value of chemical hardness, this value corresponding to the high energy gap for R_5. While a small value of chemical hardness corresponding to the low energy gap for R_4. Therefore, Au_5 the system may consider more stable, harder and less reactive, while Au_4 the system is more soft and reactive.

The value of electrophilicity enhance this sense. From the data in Table (4-1)-(4-3), the more stable systems are order as following $Cu_5 > Au_5 > Ag_5$, while the more reactive systems are order as following $Ag_4 > Cu_4 > Au_4$. Noteworthy,

the pristine double metal rings are more reactive than its counterpants of single metallic ring as given in Table (4-4). According to the computed η and S values, the reactivity of the alloyed double metallic rings increases as trends $Ag_6Au_6 > Cu_6Ag_6 > Cu_6Au_6$ (Table (4-5)).

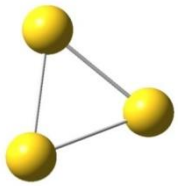
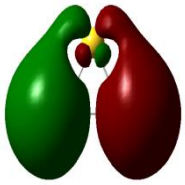
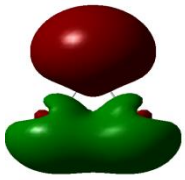
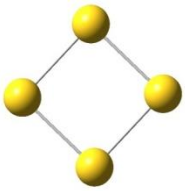
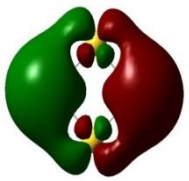
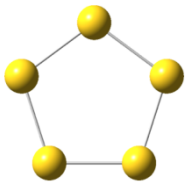
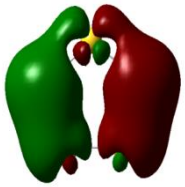
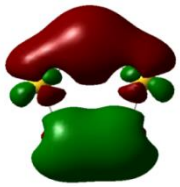
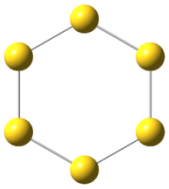
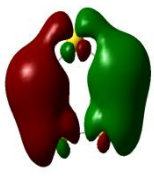
Symbol	Structure	HOMO	LUMO
(a) Au_3			
(b) Au_4			
(c) Au_5			
(d) Au_6			

Fig. (4-1): Optimized structures, and the shapes of HOMO and LUMO of Au_n (n=3-6) rings.

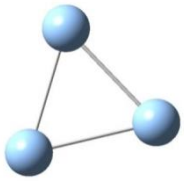
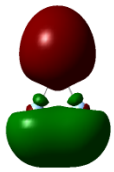
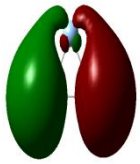
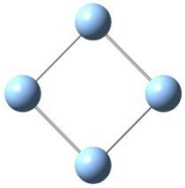
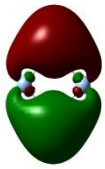
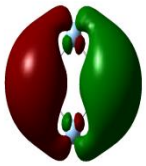
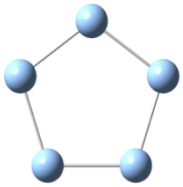
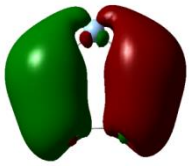
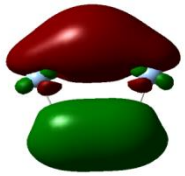
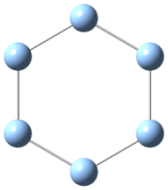
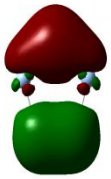
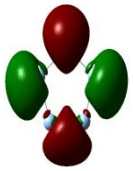
Symbol	Structure	HOMO	LUMO
(a) Ag_3			
(b) Ag_4			
(c) Ag_5			
(e) Ag_6			

Fig. (4-2): Optimized structures, and the shapes of HOMO and LUMO of Ag_n (n=3-6) rings.

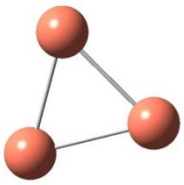
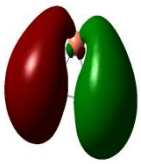
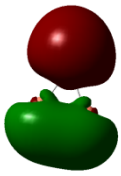
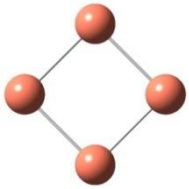
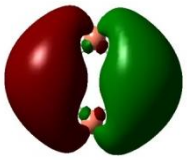
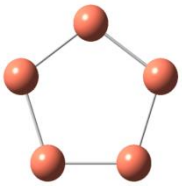
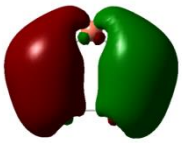
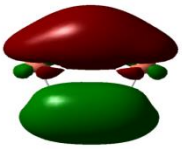
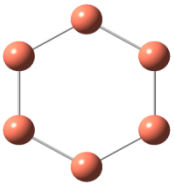
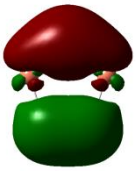
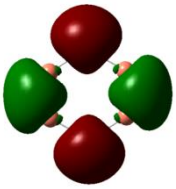
Symbol	Structure	HOMO	LUMO
(a) Cu_3			
(b) Cu_4			
(c) Cu_5			
(f) Cu_6			

Fig. (4-3): Optimized structures, and the shapes of HOMO and LUMO of Cu_n (n=3-6) rings.

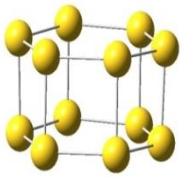
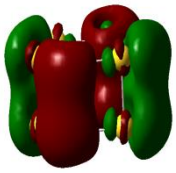
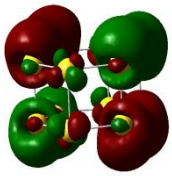
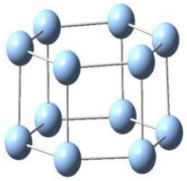
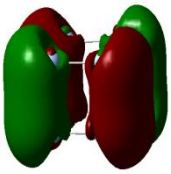
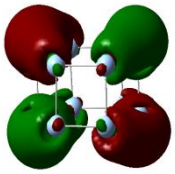
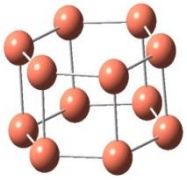
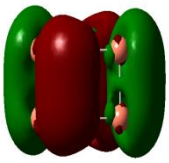
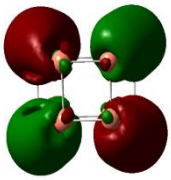
Symbol	Structure	HOMO	LUMO
(a) $2Au_6$			
(b) $2Ag_6$			
(c) $2Cu_6$			

Fig. (4-4): Optimized structures, and the shapes of HOMO and LUMO of (a)$2Au_6$, (b)$2Ag_6$ and (c)$2Cu_6$ rings.

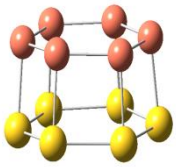
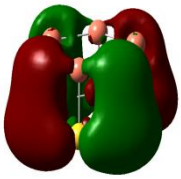
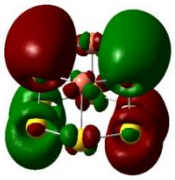
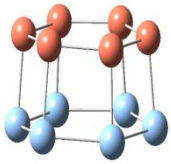
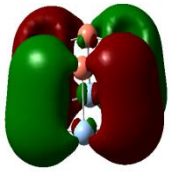
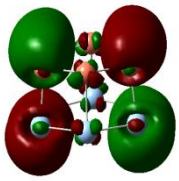
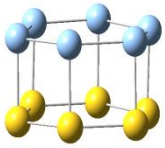
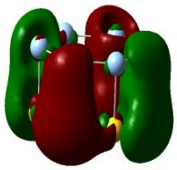
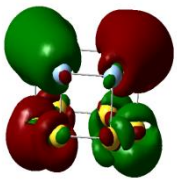
Symbol	Structure	HOMO	LUMO
(a) Cu_6Au_6			
(d) Cu_6Ag_6			
(e) Ag_6Au_6			

Fig. (4-5): Optimized structures, and the shapes of HOMO and LUMO of (a)Cu_6 Au_6, (b) Cu_6 Ag_6 and (c)Ag_6 Au_6 rings.

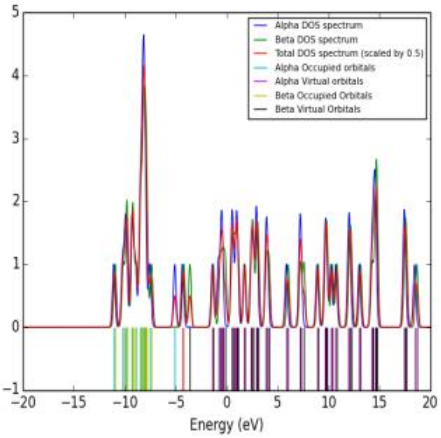
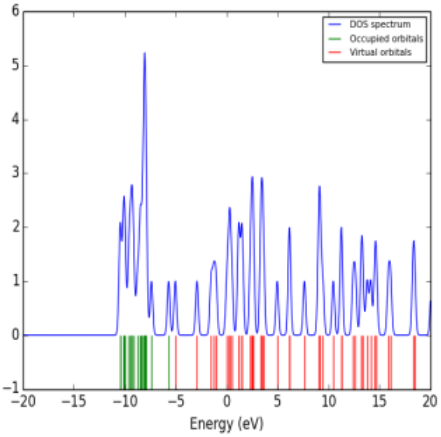
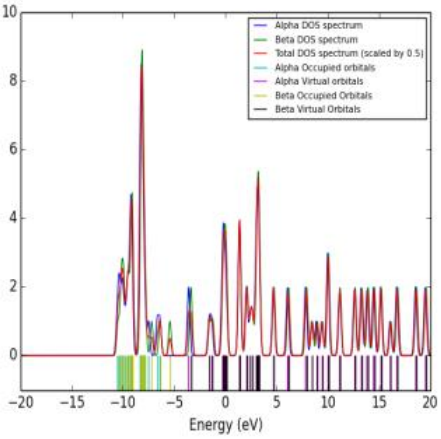
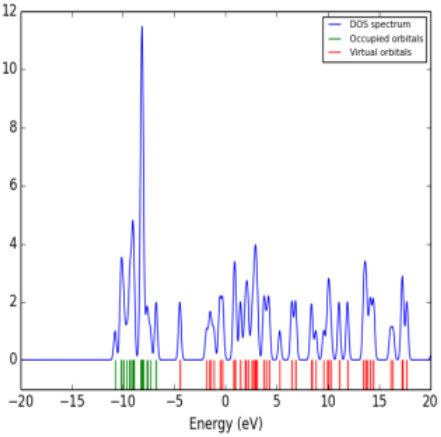
Symbol	DOS spectrum	Symbol	DOS spectrum
(a) Au_3		(b) Au_4	
(c) Au_5		(d) Au_6	

Fig. (4-6): Calculated the electronic density of states (DOS) for Au_n (n=3-6) rings.

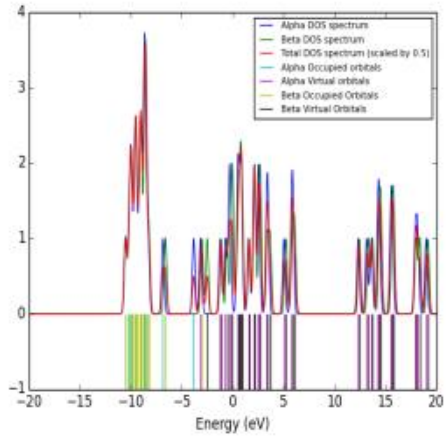
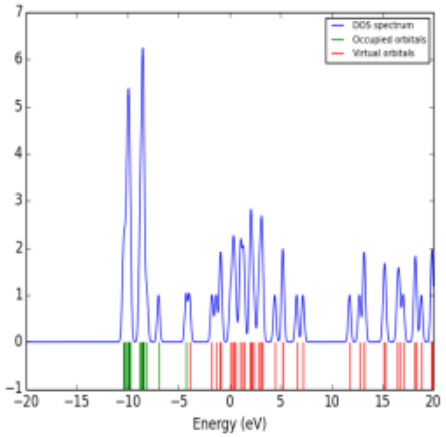
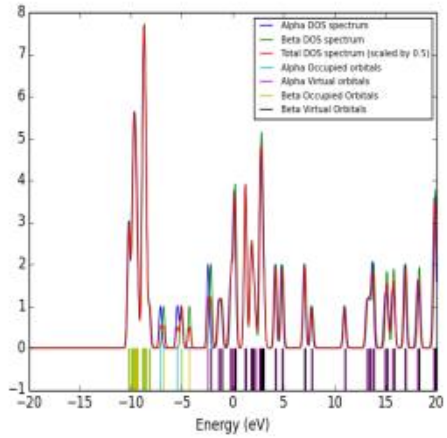
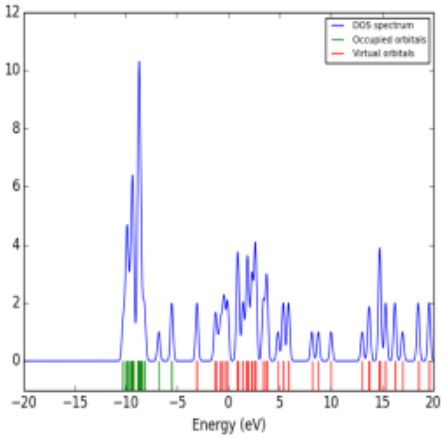
Symbol	DOS spectrum	Symbol	DOS spectrum
(a) Ag_3		(b) Ag_4	
(c) Ag_5		(d) Ag_6	

Fig. (4-7): Calculated the electronic density of states (DOS) for Ag_n (n=3-6) rings.

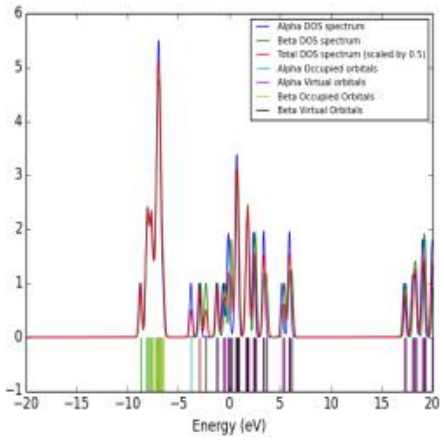
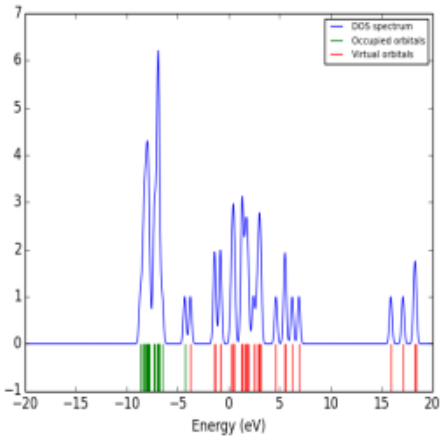
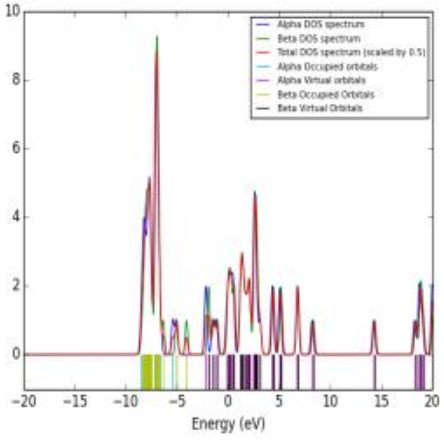
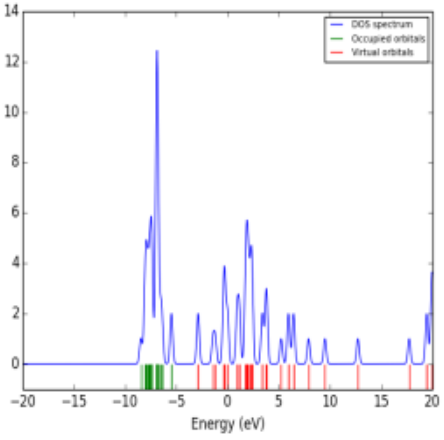
Symbol	DOS spectrum	Symbol	DOS spectrum
(a) Cu_3		(b) Cu_4	
(c) Cu_5		(d) Cu_6	

Fig. (4-8): Calculated the electronic density of states (DOS) for Cu_n (n=3-6) rings.

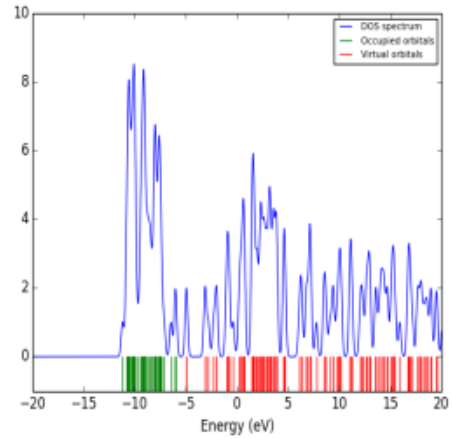
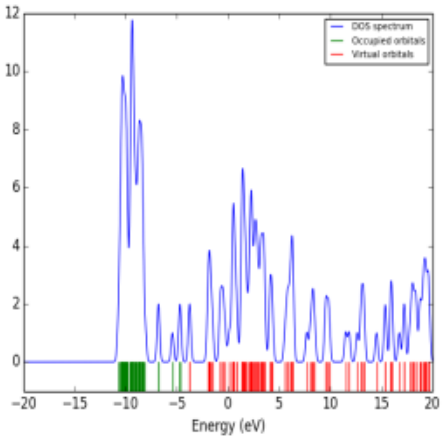
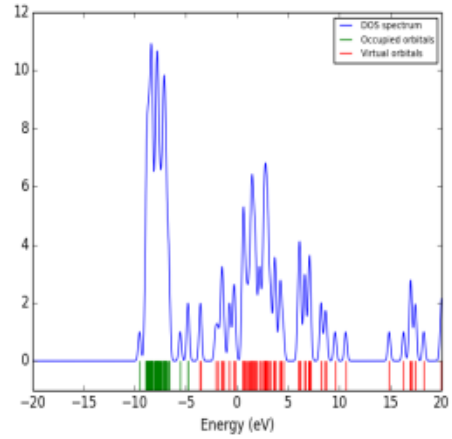
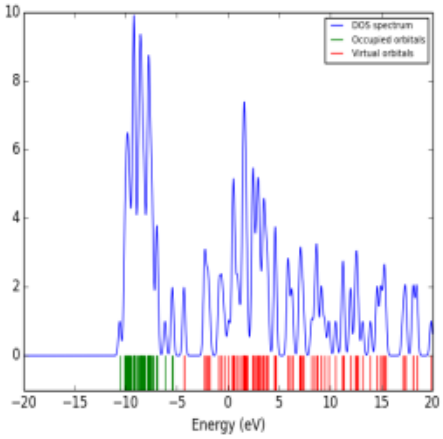
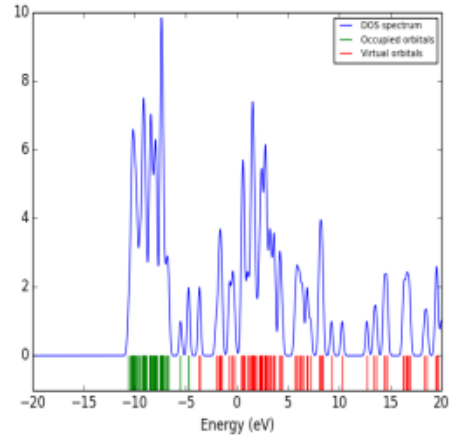
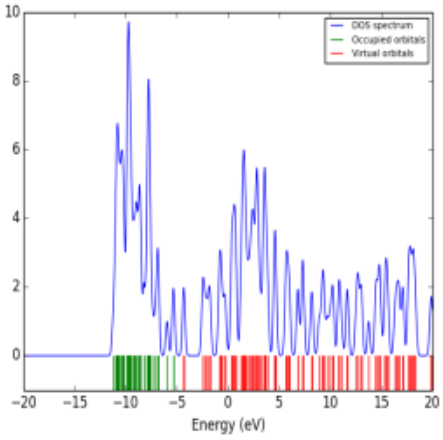
Symbol	DOS spectrum	Symbol	DOS spectrum
(a) $2Au_6$		(b) $2Ag_6$	
(c) $2Cu_5$		(d) Cu_6Au_6	
(e) Cu_6Ag_6		(f) Ag_6Au_6	

Fig. (4-9): Calculated the electronic density of states (DOS) for (a)$2Au_6$, (b)$2Ag_6$, (c)$2Cu_5$, (d)Cu_6Au_6, (e)Cu_6Ag_6 and (f)Au_6Ag_6 rings.

Table(4-1): The calculated data: HOMO, LUMO, energy, electronegativity, hardness, electrophilicity and softness of a single metallic rings (Au_3, Au_4, Au_5, Au_6).

Symbol	E_{HOMO} (eV)	E_{LUMO} (eV)	E_g (eV)	χ (eV)	η (eV)	ω (eV)	S (eV)
Au_3	-5.081	-4.334	0.747	4.707	0.373	29.659	1.338
Au_4	-5.686	-5.033	0.653	5.359	0.326	44.047	1.533
Au_5	-6.396	-3.592	2.804	4.994	1.402	8.894	0.356
Au_6	-6.764	-4.447	2.317	5.605	1.158	13.564	0.431

Table(4-2): The calculated data: HOMO, LUMO, energy, electronegativity, hardness, electrophilicity and softness of a single metallic rings (Ag_3, Ag_4, Ag_5, Ag_6).

Symbol	E_{HOMO} (eV)	E_{LUMO} (eV)	E_g (eV)	χ (eV)	η (eV)	ω (eV)	S (eV)
Ag_3	-3.812	-3.136	0.676	3.474	0.338	17.853	1.479
Ag_4	-4.270	-3.940	0.329	4.105	0.165	51.063	3.030
Ag_5	-5.046	-2.388	2.658	3.717	1.329	5.197	0.376
Ag_6	-5.522	-3.070	2.451	4.296	1.226	7.526	0.407

Table(4-3): The calculated data: HOMO, LUMO, energy, electronegativity, hardness, electrophilicity and softness of a single metallic rings(Cu_3, Cu_4, Cu_5, Cu_6).

Symbol	E_{HOMO} (eV)	E_{LUMO} (eV)	E_g (eV)	χ (eV)	η (eV)	ω (eV)	S (eV)
Cu_3	-3.749	-2.932	0.817	3.340	0.408	13.671	1.225
Cu_4	-4.299	-3.744	0.555	4.021	0.277	29.184	1.805
Cu_5	-5.050	-2.158	2.892	3.604	1.446	4.491	0.345
Cu_6	-5.471	-2.869	2.601	4.170	1.300	6.688	0.384

Table(4-4): The calculated data: HOMO, LUMO, energy, electronegativity, hardness, electrophilicity and softness of the pristine double metallic rings ($2Au_6$, $2Ag_6$, $2Cu_6$).

Symbol	E_{HOMO} (eV)	E_{LUMO} (eV)	E_g (eV)	χ (eV)	η (eV)	ω (eV)	S (eV)
$2Au_6$	-5.995	-4.940	1.055	5.467	0.527	28.356	0.948
$2Ag_6$	-4.682	-3.753	0.928	4.217	0.464	19.162	1.077
$2Cu_6$	-4.768	-3.586	1.181	4.177	0.591	14.760	0.847

Table(4-5): The calculated data: HOMO, LUMO, energy, electronegativity, hardness, electrophilicity and softness of the alloyed double metallic rings (Cu_6Au_6, Cu_6Ag_6, Ag_6Au_6).

Symbol	E_{HOMO} (eV)	E_{LUMO} (eV)	E_g (eV)	χ (eV)	η (eV)	ω (eV)	S (eV)
Cu_6Au_6	-5.421	-4.315	1.106	4.868	0.553	21.426	0.904
Cu_6Ag_6	-4.724	-3.669	1.055	4.196	0.527	16.704	0.948
Ag_6Au_6	-5.308	-4.328	0.979	4.818	0.489	23.735	1.022

Chapter Five

Conclusions and Future Works

5-1 Conclusions

1- The finite energy gap appears between two different bands of energy levels, which controlled by nearst-neighboor hopping and inter-rings coupling strengths.

2- The persistent current have vanishing behavior at integer or half-integer multiples of flux-quantum, because energy levels have either a maximum or minimum value at these values of flux.

3- The amplitudes of persistent current can be adjusted by three important parameters are in the following increasing order: $\mathrm{V} > t_{lo} > \mathrm{E}$.

4- In non-half-filled case, the amplitude of persistent current increases when the number of electrons increases.

5- The vanishing behavior of persistent current in half-filled case lead to insulating phase, while non-half filled case lead to conducting phase.

6- The persistent current decays algebraically by increasing ring size.

7- The vanishing behavior of Drude weight shows the crossing of the system from the conducting phase to the insulating phase.

8- The low-filed magnetic susceptibility have diamagnetic behavior at $\Phi \to 0$, which means only diamagnetic persistent current in the double mesoscoping ring.

9- The transverse flux controls the values of allowed quasimoment by magnitude $\frac{\Phi_t}{2}$ from through relation $\left(q = \frac{2\pi}{N}\left(n + \frac{\Phi}{\Phi_0} + \frac{1}{2}\frac{\Phi_t}{\Phi_0}\right)\right)$.

10- The PC greatly affected by the transverse flux. At on-site energies are similar, that the curvature of the PC spectrum will increase by increasing transverse flux at N_e is even, while the transverse flux lead to additionally oscillate in the PC spectrum at N_e is odd.

11- It is noted that the DOS of HOMO orbitals increase by increasing of the number of atoms in metal ring for all noble metals, due to the concentration of occupied orbitals in a narrow range of energy, while virtual orbitals are in a wide range of energy.

12- The DOS is related with the eigenenergies of the metal ring and change due to varying the number of atoms and type of material.

13- Interestingly, the most stable system is Cu_5 , while the Ag_4 system is the most effective of the other studied systems.

14- The energy gap of the studied systems exhibit semiconductor feature, which open an important new field in nanoelectronics.

15-The energy gap characteristic lead to that the pristine double metallic rings are more conductive than the alloyed double metallic rings. This result supports the result current amplitude of the rings with similar atomic sites is higher than that of the rings with different atomic sites.

5-2 Future works

1- Magneto-transport of non-interacting electrons in the triple mesoscopic ring.

2- Study the persistent current in graphene structure.

3- Investigation of electronic properties of a double binary alloy ring.

References

[1] D. Aghamalyan, M. Cominotti, M. Rizzi, D. Rossini, F. Hekking, A. Minguzzi, *et al.*, "Coherent superposition of current flows in an atomtronic quantum interference device," *New journal of Physics*, vol. 17, p. 045023, 2015.

[2] S. Saha, S. K. Maiti, and S. Karmakar, "Conformation dependent magnetotransport in a single handed helical geometry," *Physics Letters A*, vol. 379, pp. 2848-2852, 2015.

[3] H.F. Cheung, Y. Gefen, E. K. Riedel, and W.-H. Shih, "Persistent currents in small one-dimensional metal rings," *Physical Review B*, vol. 37, p. 6050, 1988.

[4] W. Rabaud, L. Saminadayar, D. Mailly, K. Hasselbach, A. Benoit, and B. Etienne, "Persistent currents in mesoscopic connected rings," *Physical Review Letters*, vol. 86, p. 3124, 2001.

[5] S. K. Maiti, "Magnetic responses in 1D mesoscopic rings and cylinders," *Physica E: Low-dimensional Systems and Nanostructures*, vol. 31, pp. 117-124, 2006.

[6] S. K. Maiti, M. Dey, S. Sil, A. Chakrabarti, and S. Karmakar, "Magneto-transport in a mesoscopic ring with Rashba and Dresselhaus spin-orbit interactions," *EPL (Europhysics Letters)*, vol. 95, p. 57008, 2011.

[7] P. Dutta and S. K. Maiti, "Magneto-transport in closed and open mesoscopic loop structures: A review," *Reviews in Theoretical Science*, vol. 3, pp. 224-243, 2015.

[8] H. Bluhm, N. C. Koshnick, J. A. Bert, M. E. Huber, and K. A. Moler, "Persistent currents in normal metal rings," *Physical review letters*, vol. 102, p. 136802, 2009.

[9] I. O. Kulik, "Persistent currents in mesoscopic loops and networks," *Turkish Journal of Physics*, vol. 27, pp. 395-418, 2004.

[10] S. Pedersen, A. E. Hansen, A. Kristensen, C. Sørensen, and P. Lindelof, "Observation of quantum asymmetry in an Aharonov-Bohm ring," *Physical Review B*, vol. 61, p. 5457, 2000.

[11] A. Alexeev, "Quantum Rings in Electromagnetic Fields," Ph. D. thesis, University of Exeter, 2013.

[12] M. Himmerich, "Persistent currents in quantum rings," Ph. D. thesis, University of mainz, 2004.

[13] A. Danilevich, "1D Quantum Rings," Ph. D. thesis, University of Erlangen-Nurnber, Germany, 2007.

[14] S. Ydman, "Magnetization dynamics in nanorings," M. Sc. thesis, University of Lunds, 2015.

[15] F. Hund, "Calculations concerning the magnetic behavior of small metallic particles at low temperatures," *Annalen der Physik*, vol. 508, pp. 1-12, 1996.

[16] J. Schrieffer, D. J. Scalapino, and J. Wilkins, "Effective tunneling density of states in superconductors," *Physical Review Letters*, vol. 10, p. 336, 1963.

[17] I. Kulik, "Magnetic flux quantization in the normal state," *Soviet Journal of Experimental and Theoretical Physics*, vol. 31, p. 1172, 1970.

[18] M. Büttiker, Y. Imry, and R. Landauer, "Josephson behavior in small normal one-dimensional rings," *Physics letters a*, vol. 96, pp. 365-367, 1983.

[19] F. C. Gethmann, "Nanosystems Out of Equilibrium: Persistent Currents and Quantum Dots," Ph. D. thesis, University of Freien, Berlin, 2012.

[20] R. Gréget, G. L. Nealon, B. Vileno, P. Turek, C. Mény, F. Ott, *et al.*, "Magnetic Properties of Gold Nanoparticles: A Room-Temperature Quantum Effect," *ChemPhysChem*, vol. 13, pp. 3092-3097, 2012.

[21] D. Sundholm, H. Fliegl, and R. J. Berger, "Calculations of magnetically induced current densities: theory and applications," *Wiley Interdisciplinary Reviews: Computational Molecular Science,* vol. 6, pp. 639-678, 2016.

[22] E. Akkermans and G. Montambaux, *Mesoscopic physics of electrons and photons*: Cambridge university press, 2007.

[23] X. Zotos and P. Prelovšek, "Transport in one dimensional quantum systems," in *Strong interactions in low dimensions*, ed: Springer, 2004, pp. 347-382.

[24] S. Gupta, S. Sil, and B. Bhattacharyya, "Fibonacci–Hubbard chain at zero and finite temperatures," *Physica B: Condensed Matter,* vol. 355, pp. 299-307, 2005.

[25] T. Heinzel, *Mesoscopic electronics in solid state nanostructures*: John Wiley & Sons, 2008.

[26] S. Datta, M. Melloch, S. Bandyopadhyay, R. Noren, M. Vaziri, M. Miller, *et al.,* "Novel interference effects between parallel quantum wells," *Physical review letters,* vol. 55, p. 2344, 1985.

[27] G. Timp, A. Chang, J. Cunningham, T. Chang, P. Mankiewich, R. Behringer, *et al.*, "Observation of the Aharonov-Bohm effect for ω c $\tau > 1$," *Physical review letters,* vol. 58, p. 2814, 1987.

[28] S. Washburn and R. A. Webb, "Aharonov-Bohm effect in normal metal quantum coherence and transport," *Advances in Physics,* vol. 35, pp. 375-422, 1986.

[29] T. Ouisse, *Electron transport in nanostructures and mesoscopic devices: an introduction*: John Wiley & Sons, 2013.

[30] A. M. de Araújo Lopes and R. A. Dias, "The Aharonov-Bohm Effect and Persistent Currents in Quantum Rings." M. Sc. Thesis, University of Aveiro, 2008.

[31] S. Ydman, "Electron-phonon dynamics in Hubbard rings and chains," B. Sc. thesis, University of Lunds, 2013.

[32] J. Sheng and K. Chang, "Spin states and persistent currents in mesoscopic rings: Spin-orbit interactions," *Physical Review B,* vol. 74, p. 235315, 2006.

[33] S. K. Maiti, "Magnetic response in 1D non-interacting mesoscopic rings: Long-range hopping in shortest path," *International Journal of Modern Physics B,* vol. 21, pp. 179-190, 2007.

[34] B.-B. Wei, S.-J. Gu, and H.-Q. Lin, "Persistent currents in the one-dimensional mesoscopic Hubbard ring," *Journal of Physics: Condensed Matter,* vol. 20, p. 395209, 2008.

[35] S. K. Maiti, "Magnetic response in mesoscopic Hubbard rings: A mean field study," *Solid State Communications,* vol. 150, pp. 2212-2217, 2010.

[36] P. Dutta, S. K. Maiti, and S. Karmakar, "Magneto-transport in a binary alloy ring," *Physics Letters A,* vol. 376, pp. 1567-1572, 2012.

[37] M. Castellanos-Beltran, D. Ngo, W. Shanks, A. Jayich, and J. Harris, "Measurement of the full distribution of persistent current in normal-metal rings," *Physical review letters,* vol. 110, p. 156801, 2013.

[38] K. Bakke and C. Furtado, "Persistent currents for a moving neutral particle with no permanent electric dipole moment," *The European Physical Journal B,* vol. 87, p. 222, 2014.

[39] M. Saha and S. K. Maiti, "Metal–insulator transition in an one-dimensional half-filled interacting mesoscopic ring with spinless fermions: Exact results," *Physics Letters A,* vol. 380, pp. 1450-1454, 2016.

[40] C. McKeever, F. Ogrin, and M. Aziz, "Dynamic susceptibility of concentric permalloy rings with opposite chirality vortices," *Journal of applied physics,* vol. 121, p. 203901, 2017.

[41] M. Filippone, C-E. Bardyn, and T. Giamarchi, "Controlled parity switch of persistent currents in quantum ladders," *Physical Review B,* vol. 97, p. 201408, 2018.

[42] E. Chu, *Discrete and continuous fourier transforms: analysis, applications and fast algorithms*: Chapman and Hall/CRC, 2008.

[43] J. M. Ziman, *Elements of advanced quantum theory*: Cambridge University Press, 1969. *and fast algorithms*: Chapman and Hall/CRC, 2008.

[44] N. Zettili, "Quantum mechanics: concepts and applications," ed: AAPT, 2003.

[45] A. Davydov, " Quantum Mechanics," ed: Oxford: Pergamon,1965

[46] P. Kapoor, J. Kumar, A. Kumar, A. Kumar, and P. Ahluwalia, "Electronic, Mechanical, and Dielectric Properties of Two-Dimensional Atomic Layers of Noble Metals," *Journal of Electronic Materials*, vol. 46, pp. 650-659, 2017.

[47] E. Y. Zarechnaya, N. V. Skorodumova, S. Simak, B. Johansson, and E. I. Isaev, "Theoretical study of linear monoatomic nanowires, dimer and bulk of Cu, Ag, Au, Ni, Pd and Pt," *Computational materials science,* vol. 43, pp. 522-530, 2008.

[48] P. Kapoor, A. Kumar, M. Sharma, J. Kumar, A. Kumar, and P. Ahluwalia, "Alloyed monolayers of Cu, Ag, Au and Pt in hexagonal phase: A comprehensive first principles study," *Materials Science and Engineering: B*, vol. 228, pp. 84-90, 2018.

[49] S. S. Shankar, A. Rai, A. Ahmad, and M. Sastry, "Rapid synthesis of Au, Ag, and bimetallic Au core–Ag shell nanoparticles using Neem (Azadirachta

indica) leaf broth," *Journal of colloid and interface science,* vol. 275, pp. 496-502, 2004.

[50] H. Huang and F. Spaepen, "Tensile testing of free-standing Cu, Ag and Al thin films and Ag/Cu multilayers," *Acta Materialia,* vol. 48, pp. 3261-3269, 2000.

[51] V. Ozoliņš, C. Wolverton, and A. Zunger, "Cu-Au, Ag-Au, Cu-Ag, and Ni-Au intermetallics: First-principles study of temperature-composition phase diagrams and structures," *Physical Review B,* vol. 57, p. 6427, 1998.

[52] X-D. Kai-Xiong and J. Hong, "Application of Gaussian03/GaussView in NMR spectroscopy teaching," *Chinese Journal of Spectroscopy Laboratory*, vol. 1, p. 058, 2012.

[53] F. N. Ajeel, "Analytical Insight into the Effect of Electric Field on Molecular Properties of Homonuclear Diatomic Molecules," *Current Smart Materials,* vol. 2, pp. 153-161, 2017.

[54] P. J. Hay and W. R. Wadt, "Ab initio effective core potentials for molecular calculations. Potentials for the transition metal atoms Sc to Hg," *The Journal of chemical physics*, vol. 82, pp. 270-283, 1985.

[55] P. J. Hay and W. R. Wadt, "Ab initio effective core potentials for molecular calculations. Potentials for K to Au including the outermost core orbitals," *The Journal of Chemical Physics,* vol. 82, pp. 299-310, 1985.

[56] A. D. Becke, "Density-functional thermochemistry. III. The role of exact exchange," *The Journal of chemical physics,* vol. 98, pp. 5648-5652, 1993.

[57] C. Lee, W. Yang, and R. G. Parr, "Development of the Colle-Salvetti correlation-energy formula into a functional of the electron density," *Physical review B,* vol. 37, p. 785, 1988.

[58] M. Oftadeh, S. Naseh, and M. Hamadanian, "Electronic properties and dipole polarizability of thiophene and thiophenol derivatives via density

functional theory," *Computational and Theoretical Chemistry*, vol. 966, pp. 20-25, 2011.

[59] A. D. Becke, "Density-functional exchange-energy approximation with correct asymptotic behavior," *Physical review A*, vol. 38, p. 3098, 1988.

[60] W. Kohn, A. D. Becke, and R. G. Parr, "Density functional theory of electronic structure," *The Journal of Physical Chemistry*, vol. 100, pp. 12974-12980, 1996.

[61] C. J. Cramer, *Essentials of computational chemistry: theories and models*: John Wiley & Sons, 2013.

[62] S. S. Li, *Semiconductor physical electronics*: Springer Science & Business Media, 2012.

[63] A. D. McNaught and A. Wilkinson, "Compendium of chemical terminology. Vol. 1669," ed: Oxford: Blackwell Science, 1997.

[64] F. Jensen, *Introduction to computational chemistry*: John wiley & sons, 2017.

[65] C. L. Tang, *Fundamentals of quantum mechanics: for solid state electronics and optics*: Cambridge University Press, 2005.

[66] W. G. Cochran, *Sampling techniques*: John Wiley & Sons, 2007.

[67] R. Gotwals and S. Sendlinger, "A Chemistry Educator's Guide to Molecular Modeling," *The North Carolina School of Science and Mathematics, Durham, NC*, 2007.

الخلاصة

العمل الحالي هو دراسة نظرية للخواص الألكترونية لحلقة ميزوسكوبية مزدوجة معرضة لفيض أهارونوف-بوهم. يتألف النظام المأخوذ بنظر الاعتبار في هذه الدراسة من حلقتين مربوطتين بشكل متوازي, بنوعين مختلفين من المواقع الذرية.

يتضمن هذا العمل جزأين. الجزء الأول هو دراسة تحليلية لطيف الطاقة والتيار الدائم ووزن درود والتأثرية المغناطيسية منخفضة المجال لحلقة ميزوسكوبية مزدوجة بواسطة طريقة الربط المشدود. تم حساب الخواص الألكترونية بوجود وعدم وجود الفيض المستعرض. تبين النتائج التحليلية بأن الطاقات الموقعية لكلا نوعي الذرات وقوى الإزدواج ما بين الحلقات وقوى القفز لأقرب جوار والفيض المستعرض تلعب دور مهم في ضبط الخواص الألكترونية للنظام تحت الدراسة.

الجزء الثاني هو محاكاة وإكمال للخواص الألكترونية المدروسة في الجزء الأول. يعتبر هذا الجزء دراسة حاسوبية للخواص الألكترونية للحلقات المعدنية في حالاتها الألكترونية الأرضية بواسطة نظرية دالة الكثافة (DFT) , التي أنجزت بواسطة برنامج الكاوسين 09W .الحلقات المعدنية المدروسة في الجزء الثاني هي حلقة معدنية مفردة وحلقة معدنية مزدوجة نقية وحلقة معدنية مزدوجة مشوبة من المعادن النبيلة الذهب والنحاس والفضة. تتكون الحلقة المعدنية المفردة من عدد ذرات (3-6). تم تصميم الحلقة المعدنية المزدوجة النقية من حلقتين بنفس المعدن, كل حلقة تتضمن 6 ذرات. بينما صممت الحلقة المعدنية المزدوجة المشوبة من حلقتين بمعادن متباينة. الهندسية الأفضل وأعلى مدار جزيئي مشغول (HOMO) وأوطئ مدار جزيئي فارغ (LUMO) وفجوة الطاقة والكهروسالبية والألفة الألكترونية والصلادة الكيميائية والمطاوعة الكيميائية تبين أن الأنظمة المدروسة لها خاصية شبه الموصل.

جمهورية العراق
وزارة التعليم العالي والبحث العلمي
جامعة ذي قار / كلية العلوم
قسم الفيزياء

التركيب الالكتروني وخواص نقل الالكترون في الحلقات الميزوسكوبيه المزدوجه

رسالة مقدمة الى مجلس كلية العلوم-جامعة ذي قار وهي جزء من متطلبات نيل درجة ماجستير في علوم الفيزياء

من قبل

سمر مزهر مرداس

بكالوريوس علوم فيزياء – جامعة ذي قار 2010

بأشراف

أ.م.د. لافي فرج البدري ***أ.د. فلاح حسن الأسدي***

1439 هـ 2018 م